Three-dimensional structural modeling of an active fault zone based on complex outcrop and subsurface data: The Middle Durance Fault Zone inherited from polyphase Meso-Cenozoic tectonics (southeastern France)

Cédric Guyonnet-Benaize, Juliette Lamarche, Fabrice Hollender, Sophie Viseur, Philippe Munch, Jean Borgomano

AGU PUBLICATIONS

Tectonics

RESEARCH ARTICLE
10.1002/2014TC003749

Key Points:
- New 3-D geological model of the deep basin structure of the Middle Durance region
- MDFZ is a transfer fault

Correspondence to:
C. Guyonnet-Benaize,
cedric.guyonnet-benaize@hotmail.fr

Citation:
Guyonnet-Benaize, C., J. Lamarche, F. Hollender, S. Viseur, P. Münch, and J. Borgomano (2015), Three-dimensional structural modeling of an active fault zone based on complex outcrop and subsurface data: The Middle Durance Fault Zone inherited from polyphase Meso-Cenozoic tectonics (southeastern France), *Tectonics*, *34*, 265–289, doi:10.1002/2014TC003749.

Received 29 SEP 2014
Accepted 30 DEC 2014
Accepted article online 7 JAN 2015
Published online 20 FEB 2015

Three-dimensional structural modeling of an active fault zone based on complex outcrop and subsurface data: The Middle Durance Fault Zone inherited from polyphase Meso-Cenozoic tectonics (southeastern France)

Cédric Guyonnet-Benaize[1], Juliette Lamarche[2], Fabrice Hollender[1,3], Sophie Viseur[2], Philippe Münch[4], and Jean Borgomano[5]

[1]French Alternative Energies and Atomic Energy Commission, Saint-Paul-les-Durance, France, [2]Technopôle de l'Environnement Arbois-Méditerranée, Aix-Marseille Université, CNRS, IRD, UM34-CEREGE, Aix-en-Provence, France, [3]Institut des Sciences de la Terre, Université Grenoble, CNRS, IRD, Grenoble, France, [4]Géosciences Montpellier, UMR 5243 Université Montpellier 2, Montpellier, France, [5]TOTAL Exploration and Production, Pau, France

Abstract The objective of this study was to realize a three-dimensional (3-D) geological model of the deep basin structure of the Middle Durance region (of folds and faults) by integration of geological and geophysical data, and to evaluate its fault geometry and tectonic history. All of the available geophysical and geological data were compiled in three dimensions using the gOcad geomodeler. The geological and geophysical data were used to build a 3-D geological model of the Middle Durance region. The data on the 3-D geometry of fault surfaces and stratigraphic horizons and the thickness maps of the main stratigraphic units are supported by the 3-D geological model. We show that the Middle Durance Fault cannot be interpreted as a single fault plane that affected the entire Meso-Cenozoic sedimentary layers and the Paleozoic basement but as a listric segmented faulting system in sedimentary layers, rooted in Triassic evaporites and a normal block faulting system in the basement. This decoupling level in the Triassic layers reveals thin-skin deformation, formed by strong mechanical decoupling between the Mesozoic sedimentary cover and the Paleozoic basement. This study also confirms that the Provence geological structure has resulted mainly from Pyrenean deformation, which was partly reactivated by Alpine deformation. We demonstrate that the Middle Durance Fault Zone is a transfer fault that accommodates deformation of the sedimentary filling of the South-East Basin through modified fold geometry over a zone of 7 km to 8 km around the main segment of the fault zone.

1. Introduction

Earthquake ruptures and the subsequent seismogenic potential are controlled in part by the geometric complexity of the relevant faults [*Wells and Coppersmith*, 1994; *Cushing et al*., 2005]. Although detailed mapping of fault traces and microstructural investigations can unravel some of the complexities, these often lack clear investigations into the segmentation and three-dimensional (3-D) geometry of fold and fault systems at depth. Such studies generally result in nonunique assessments of the folds and fault geometries at the crustal scale, which are poorly validated by complementary deep geophysical imaging. These ideal conditions are met in the Middle Durance valley of southeastern France. This region is located on the southeastern border of the South-East (SE) Basin, which is characterized by an active fault zone oriented NE-SW, called the Middle Durance Fault Zone (MDFZ), with its associated E-W thrusts and folds (Figure 1).

The hydrocarbon potential of the SE Basin and the tectonic activity of the MDFZ have stimulated numerous stratigraphic, tectonic, and seismological studies of the Middle Durance Valley area [*Roure et al*., 1992; *Benedicto Esteban*, 1996; *Roure and Colletta*, 1996; *Cushing and Bellier*, 2003; *Cushing et al*., 2004; *Guignard et al*., 2005; *Bellier et al*., 2007; *Cushing et al*., 2008; *Molliex*, 2009; *Le Pichon et al*., 2010; *Rangin et al*., 2010; *Molliex et al*., 2011]. Extensive seismic reflection surveys conducted by oil companies between 1971 and 1986 were mainly based on geophysical data [*Baudrimont and Dubois*, 1977; *Debrand-Passard et al*., 1984; *Bove*, 1996, 1997, 1998], while some studies were focused on the deep structure and the stratigraphic and tectonic evolution of the SE Basin [*Benedicto Esteban*, 1996; *Cushing et al*., 2004; *Le Pichon et al*., 2010; *Rangin et al*., 2010;

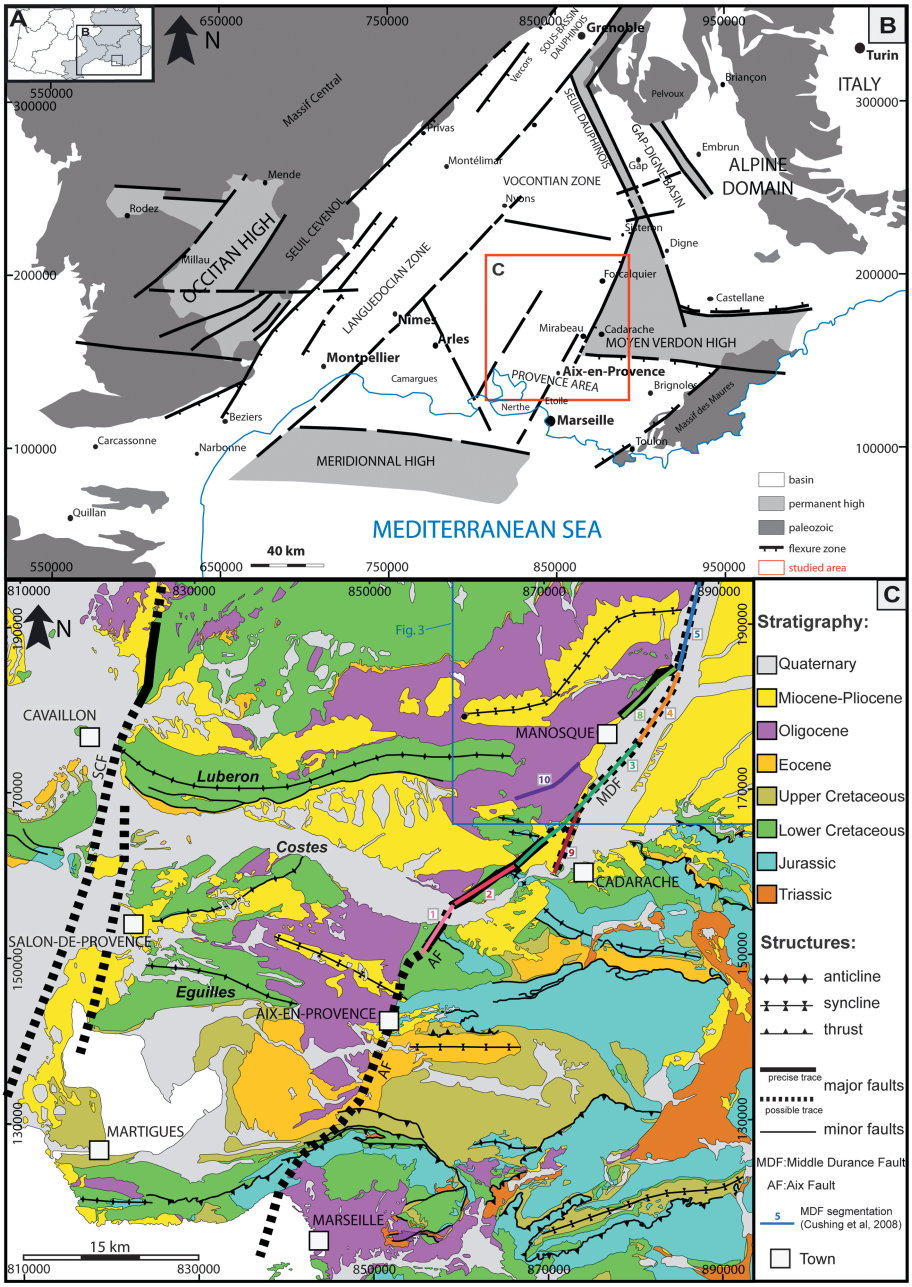

Figure 1. Structural sketch of Provence (modified from Provence geological map, 1:25 000[e], BRGM, 1977). (a) Map of southeastern France, indicating Provence. (b) Expanded from box B in Figure 1a, showing the main tectonic accidents of the SE Basin. (c) Expanded from box C in Figure 1b, showing the structural sketch of the Middle Durance area, with the main faults and folds.

Molliex et al., 2011]. These studies evaluated the thickness of the Meso-Cenozoic sedimentary units, and they tried to image the depth of the Paleozoic basement. Other studies were focused on the segmentation, deep geometry, and seismogenic activity of the MDFZ and its associated folds [*Cushing et al.*, 2004].

In the case of the tectonic structure of the Middle Durance region, many questions remain unresolved, such as the following: What are the relationships between the Paleozoic basement and the Meso-Cenozoic filling of the SE Basin? How (and where) do these sediments accommodate deformation? What are the sedimentary layers and the tectonic structures that accommodate this deformation? What is the real 3-D geometry of the complex MDFZ? What is the effective role of the MDFZ in accommodating of this

deformation? What are the structural relationships between this major fault and the main tectonic structures (e.g., the E-W folds and thrusts)?

In our study, we focus on the importance of the MDFZ in accommodating deformation, fault reactivation, and décollement levels. We characterize with greater precision the deep geometry of the MDFZ and its associated folds (e.g., ramp geometry, *décollement* level depth, and geometric link with the MDFZ). Indeed, an understanding of the realistic 3-D deep structure of the Middle Durance region and the structural relationships between the segmentation of the MDFZ and its associated folds and fault geometry is of paramount importance for the prediction of earthquake ruptures. To achieve this goal, we carry out 3-D structural modeling, including the actual 3-D geometry of the MDFZ and the main regional tectonic structures. We realize a 3-D model that will help seismologists to produce ground-motion simulations that will allow us to better understand and characterize the seismic risk assessment in the case of civil or nuclear building engineering.

2. The Geological Setting

2.1. Regional Geology

The study was carried out in the Middle Durance region in the southeastern corner of the SE Basin (Provence, southeastern France; Figure 1). The tectonic and sedimentary evolution of this region has been punctuated by successive tectonic events from Mesozoic to Cenozoic times (Figure 2).

From Triassic to Early Cretaceous times, intracontinental rifting led to strong subsidence and the opening of the Alpine Tethys [*Boillot et al*., 1984; *Lemoine*, 1985; *Lemoine et al*., 1986; *Lemoine and De Graciansky*, 1988], which was characterized in the SE Basin by siliciclastic and evaporitic (Triassic), marly and marly-limestone (Jurassic), and limestone (Lower Cretaceous) deposits. During the Cretaceous, this region was affected by regional uplift, known as the "mid-Cretaceous Durance" uplift [*Masse and Philip*, 1976; *Guyonnet-Benaize et al*., 2010], which was characterized by the emersion and the partial erosion of the Late Jurassic and Early Cretaceous carbonates and by the formation of bauxite.

From Middle Cretaceous to Eocene, a tectonic inversion affected the SE Basin, which was located in the foreland of the Pyrenean orogeny at that time [*Corroy et al*., 1964; *Choukroune et al*., 1973; *Choukroune and Mattauer*, 1978; *Arnaud*, 1981; *Tempier*, 1987; *Rosenbaum et al*., 2002]. In the Middle Durance region, this compression resulted in north-verging E-W folds and thrust faults (e.g., Luberon, Costes, and Eguilles; Figure 2).

From Late Eocene to Early Miocene, the West European and Liguro-Provencal rifting [*Triat and Truc*, 1983; *Gattacceca et al*., 2007] affected southeastern France and were responsible for the development of grabens and pull apart minibasins (Figure 2). In the Middle Durance region, minibasins such as the Manosque-Forcalquier Oligocene basin have deeply subsided and been filled by kilometer-thick Oligocene deposits. More recently, during the Miocene, the Alpine compression reactivated the preexisting Pyrenean folds and thrusts [*Combes*, 1984; *Faucher et al*., 1988; *Gidon and Pairis*, 1992; *Ford and Stahel*, 1995; *Laurent et al*., 2000; *Leleu*, 2005; *Espurt et al*., 2012; *Molliex et al*., 2011; *Lamarche et al*., 2012; *Gisquet et al*., 2013; *Lavenu et al*., 2013].

2.2. The Structural Pattern of the Middle Durance

The Provence region corresponds to the southeastern corner of the much wider SE Basin (Figure 1). This region is bounded by Paleozoic structural basement highs: the Meridional high to the south, the Moyen Verdon high to the north, and the Maures massif to the south-east. The area is crosscut by NNE-SSW transfer faults (Middle Durance Fault (MDF), Aix Fault (AF), and Salon-Cavaillon Fault; Figure 1c) [*Molliex et al*., 2011] which were inherited from Paleozoic basement faults [*Arthaud and Matte*, 1977]. In the present study, we focus on the MDFZ, in a wide sense, which also includes the AF.

The present-day structural pattern of the Provence area is the result of successive tectonic events (see section 2.1 and Figure 2). In the study area, the thickness of the Meso-Cenozoic sedimentary cover is highly variable on both sides of the MDFZ. In the western part of the MDFZ, the sedimentary series was affected by continuous subsidence through Mesozoic times, when it reached a thickness of 10 km, whereas in the eastern part of the MDFZ, it does not exceed a thickness of 2 km [*Grellet et al*., 1993; *Benedicto Esteban*, 1996; *Chantaine et al*., 1996; *Le Pichon et al*., 2007]. The structure of the Middle Durance region is characterized by

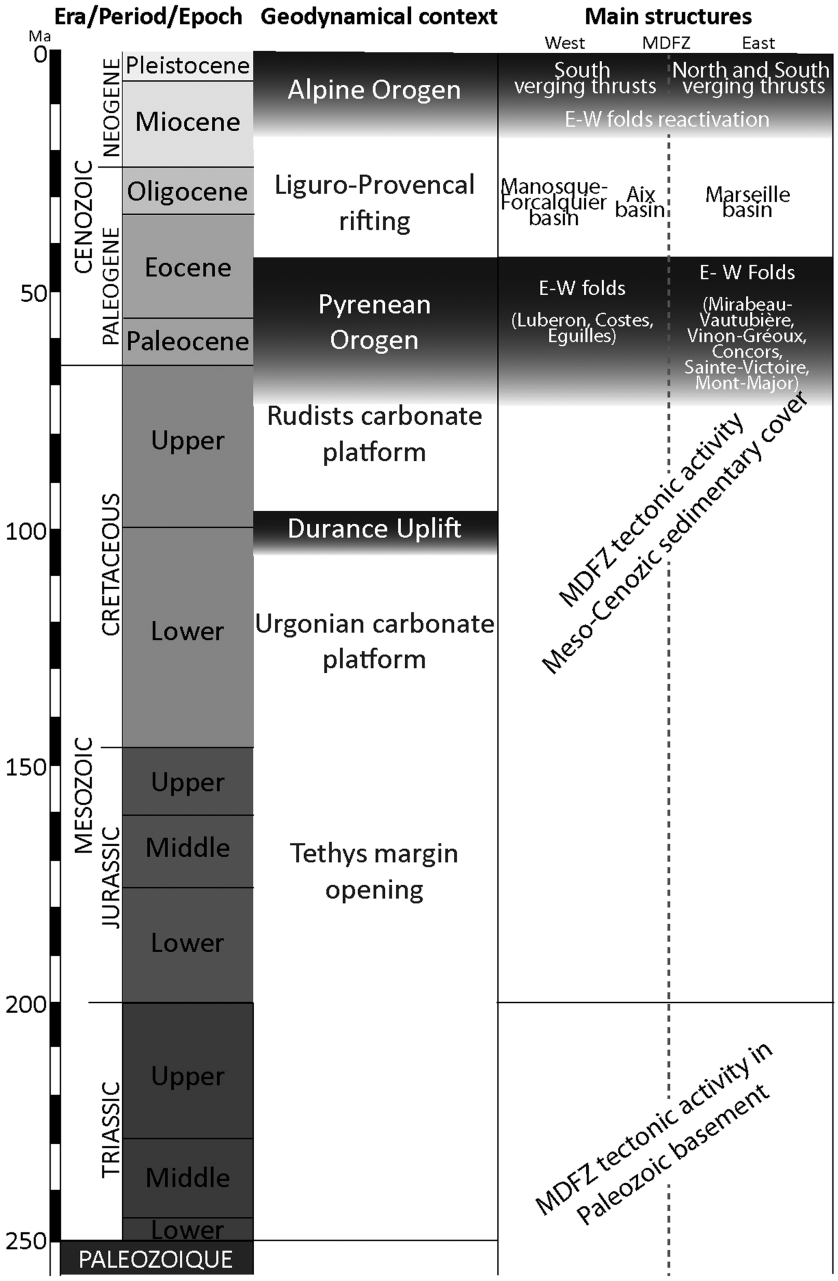

Figure 2. Main tectonic events and associated structures since the Mesozoic times.

E-W folds and thrusts (e.g., to the West of the MDFZ: Luberon, Costes, and Nerthe; to the East of the MDFZ: Greoux-Vinon, Mirabeau-Vautubière, Concors, and Ste Victoire; Figure 1c) that are separated by wide and flat areas, the tectonic deformation of which has been moderate or limited (e.g., Viens, Cucuron, Valensole, Cadarache, and Arc). In the western part of the MDFZ, the E-W folds and thrusts are bounded by the NNE-SSW Middle Durance, Aix, and Salon-Cavaillon transfer faults (Figure 1c).

2.3. Structural and Kinematic Context of the Middle Durance Fault Zone

2.3.1. Subsurface Geometry of the Middle Durance Fault Zone

The MDFZ separates two different structural regions to the east and the west, and it is 80 km long and can be subdivided into two parts: a deep part in the Paleozoic basement that is characterized by a staircase geometry that affects the top basement; and a shallow part in the Meso-Cenozoic sedimentary layers.

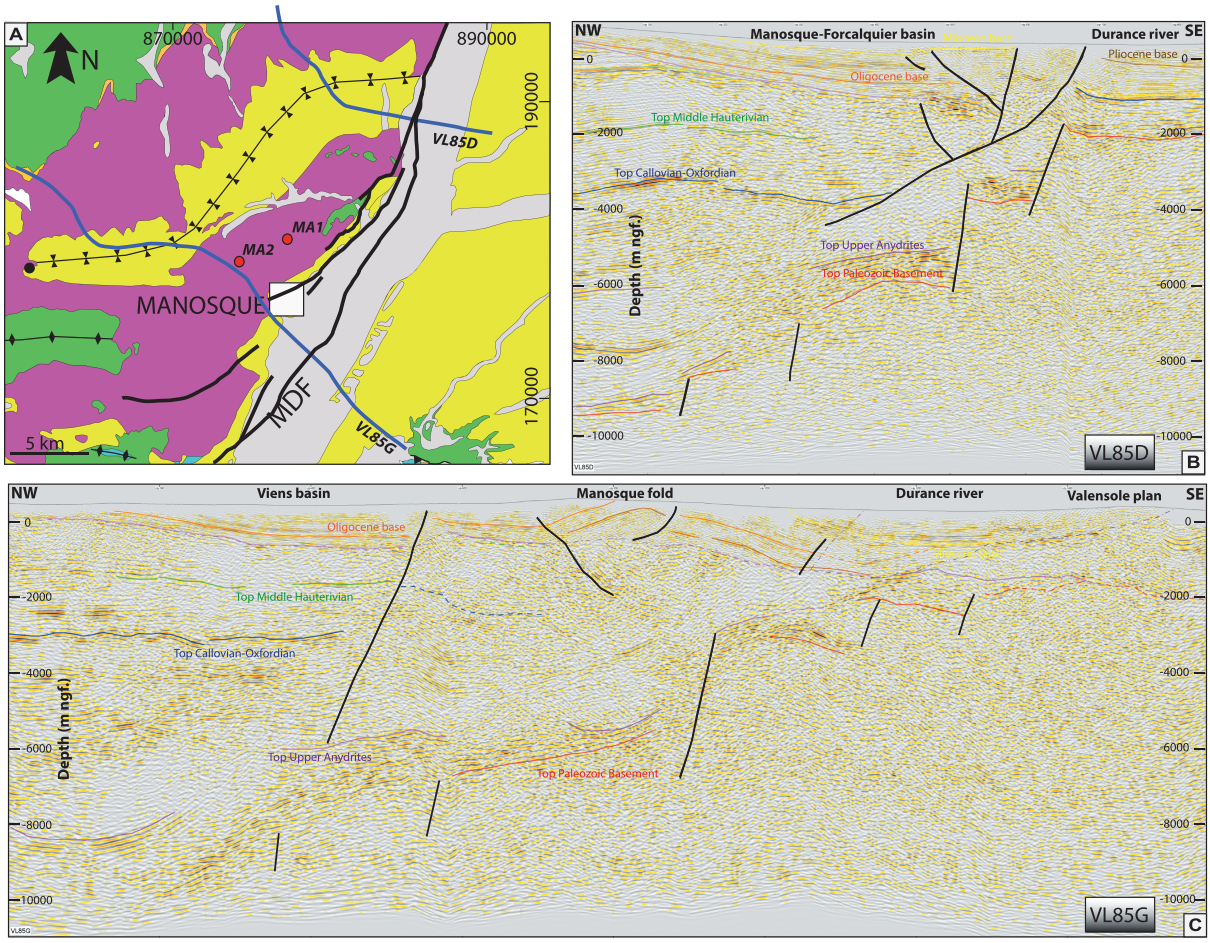

Figure 3. (a) Seismic imagery of the Paleozoic basement and the Meso-Cenozoic sedimentary layers of the Middle Durance region (see Figure 2), illustrating the MDF geometry and the locations of the deep drilling of Manosque 1 (MA1) and Manosque 2 (MA2). Seismic views of the interpretations of the (b) VL85D and (c) VL85G profiles. Location of these profiles is in box A.

This shallow part of the MDFZ is characterized by a listric geometry with reverse movement, which dips (60° to 70°) to the west. At a depth of 5 km to 6 km, the listric fault is horizontal, and it reaches a décollement level in the Triassic evaporites. Thus, the 3-D geometry of the MDFZ is complex and has not been precisely described yet.

2.3.2. Tectonic History of the Middle Durance Fault Zone

The kinematic reconstruction of the MDFZ tectonic activity indicates four alternating extensional and compressional tectonic episodes that have been interpreted from deep drilling and seismic reflection profiles [*Hollender et al*., 2009] (Figure 3) as follows:

1. The first episode resulted from extension, and it was associated with normal dip-slip faults that affected the Paleozoic basement. This episode occurred during the Triassic-Late Jurassic interval, in relation to the edification of the Alpine Tethys European passive margin [*Baudrimont and Dubois*, 1977].
2. The second episode resulted from compression, and it was associated with inverse dip-slip faults that affected the Upper Cretaceous to Paleogene sedimentary series, in relation to the Pyrenean orogeny [*Benedicto Esteban*, 1996; *Roure and Colletta*, 1996; *Cushing et al*., 2008].
3. The third episode resulted from extension, and it was associated with normal dip to strike-slip faults that affected the Oligocene to Miocene sedimentary series, in relation to the west European rifting [*Bergerat*, 1987].
4. The fourth episode resulted from compression (of Alpine orogeny), and it was associated with inverse dip-slip faults that affected the Miocene to present-day sedimentary series, in relation to the Alpine orogeny [*Baroux et al*., 2001; *Cushing et al*., 2008].

Table 1. Available Geological and Geophysical Surface and Subsurface Data of the Middle Durance Region

Data Type	Scale	Reference/Date
	Surface Data	
Geological Maps BRGM		
Carpentras (941)	1:50 000	*Blanc et al.* [1975]
Sault-de-Vaucluse (942)	1:50 000	*Blanc and Rouire* [1973]
Forcalquier (943)	1:50 000	*Gigot et al.* [1982]
Cavaillon (967)	1:50 000	*Germain et al.* [1966]
Reillane (968)	1:50 000	*Belleville et al.* [1966]
Manosque (969)	1:50 000	*Mercier et al.* [1972]
Salon-de-Provence (994)	1:50 000	*Gouvernet et al.* [1968]
Pertuis (995)	1:50 000	*Arlhac et al.* [1970]
Tavernes (996)	1:50 000	*Mennessier and Modret* [1966]
Martigues-Marseille (1020)	1:50 000	*Lutaud and Denizot* [1963]
Aix-en-Provence (1021)	1:50 000	*Denizot et al.* [1959]
Brignoles (1022)	1:50 000	*Mennessier et al.* [1979]
Punctual outcrop observations	Metric to centimetric	*Guyonnet-Benaize* [2011]
Topographic maps	1:25 000	*IGN* [1998]
Digital elevation model	50 m sampled	*IGN* [1998]
	Subsurface Data	
Oil Boreholes	Metric	BEPH database
Geotechnical boreholes	Metric to centimetric	CEA database
Seismic profiles	Second	BEPH database
Balanced cross sections	1:50 000	*Guyonnet-Benaize* [2011]

2.3.3. Surface Traces of the Middle Durance Fault Zone

The MDFZ segmentation consists of a branching fault system that is part of a relay zone between the northern area (i.e., the Middle Durance area sensu stricto) and the south (i.e., the AF area). In the study area, the fault mapping indicated eight segments from north to south, as described by *Terrier* [2004a, 2004b] and *Cushing et al.* [2008] (Figure 1, segments 1, 2, 3, 4, 5, 8, 9, and 10). These segments strike NE-SW (N40°), except for the relay zone (N90°) [*Guignard et al.*, 2005], with an average length of between 6.5 km and 14 km [*Terrier*, 2004a, 2004b]. In the northern part of the study area, the MDFZ (Figure 1, segments 4, 5, and 8) might be linked to the Luberon thrust fold [*Chardon and Bellier*, 2003; *Guignard et al.*, 2005] by segment 10 (Figure 1). The south termination of the MDFZ (Figure 1, segments 3 and 9) is connected to the AF (Figure 1, segment 1) by a relay zone (Figure 1, segment 2).

3. The Database

The goal of the present study was to establish the construction of a geological model of the 3-D deep structure of the Middle Durance region, and to understand the structural relationships between the segmentation of the MDFZ and its associated folds and fault geometry. To achieve this goal, we collected and compiled all of the available geological and geophysical surface and subsurface data, which were then integrated into three dimensions to realize a 3-D geological model of the Middle Durance region (Table 1). This data set is characterized by high heterogeneity (e.g., outcrop measurements, wells, seismic reflection lines, and cross sections), as presented below.

3.1. Surface Data

The surface data are georeferenced punctual measurements of outcrops and georeferenced data extracted from geological maps (Figure 4). Geological boundaries observed in the field, such as fault traces or stratigraphic limits, are used to constrain the near-surface geometry of the subsurface faults and the interpretation of the stratigraphic horizons of the seismic reflection profiles and cross sections. The data on punctual outcrops included 94 measurements of the bed attitude and thickness, and these were used to constrain the subsurface geometry. The data were mostly collected along seismic reflection profiles and cross sections, although we tried to obtain a relatively representative distribution of the surface data in the Middle Durance region. Each measurement was georeferenced. The geological maps used were 12 maps (1:50,000^{e} scale) from BRGM (Bureau de Recherche Géologiques et Minières, http://www.brgm.fr/) over the

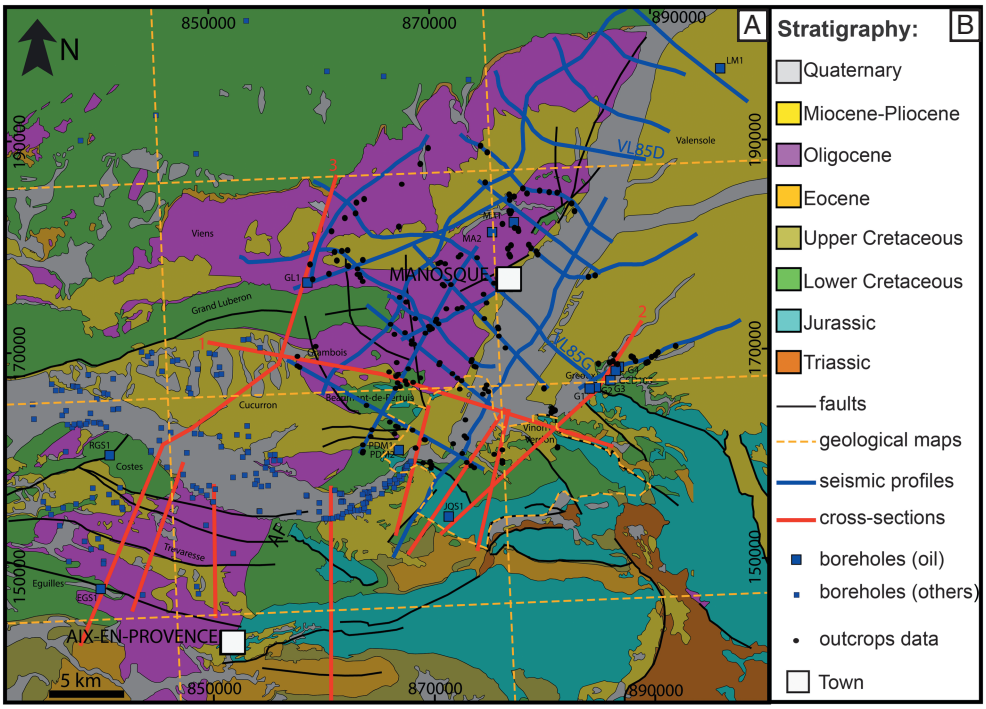

Figure 4. (a) One-dimensional and two-dimensional data location on the Middle Durance geological map. (b) Stratigraphy of the Middle Durance region and nature of 1-D (boreholes and outcrops) and 2-D (seismic profiles and cross sections) data used for three-dimensional modeling.

50 km × 70 km study area and two detailed geological maps centered on the Cadarache valley (1:25,000^e and 1:5,000^e scales) [*Borgomano et al.*, 2010] over an area of 80 km^2. The outcrop measurements and geological maps were projected onto a topographic map (1:25,000^e scale) and a digital elevation model (DEM) with 25 m resolution, both of which were provided by the IGN (Institut Géographique National, http://www.ign.fr/).

3.2. Subsurface Data

The subsurface data comprised wells and industrial seismic reflection lines. Fourteen boreholes with well logging (i.e., sonic, density, and resistivity) were used in this study (Figure 4). These boreholes were extracted from the BEPH (Bureau Exploration-Production des Hydrocarbures, http://www.beph.net/) database: Five boreholes were located west of the MDFZ (Manosque 1, 2; Grand Luberon 1; Rognes 1; and Eguilles 1), seven east of the MDFZ (Les Mées 1, Greoux CD105, 1, 2, 3, and 4, and Jouques 1), and two close to the MDFZ (Pont-de-Mirabeau 1 and 2). The boreholes had a total depth (true depth) of 398 m to 5385 m (Table 2).

The boreholes west of the MDFZ were mainly drilled in Neogene and Paleogene siliciclastic sediments and Cretaceous and Jurassic limestones. To the east of the MDFZ, the boreholes were drilled in Quaternary, Neogene, and Paleogene siliciclastic sediments and Cretaceous, Jurassic, and Triassic limestones. Three of these reached the Paleozoic basement, with an average depth of 2100 m: Greoux 1 (1810 m), Jouques (2476 m), and Les Mées (1760 m). In addition, 189 geotechnical boreholes were extracted from the BRGM database (BSS, Banque de Données du Sous-Sol, http://www.brgm.fr/; Figure 4). These boreholes reached shallow depths, down to 250 m.

The seismic reflection lines studied were acquired between 1971 and 1986 by the oil companies. The raw data of 21 seismic reflection sections (along 381 km) were reprocessed by the French Alternative Energies and Atomic Energy Commission (CEA; Cashima Research Project, CEA Cadarache) in collaboration with the BRGM, using state-of-the-art seismic signal processing. Most of the seismic reflection lines trended in the NW-SE direction (Figure 4), while a few lines trended in the NE-SW direction. These sections were interpreted collectively by a wide panel of geophysicists and structural geologists from different research institutes and companies (CEA, Institut de Radioprotection et de Sûreté Nucléaire (IRSN), Centre Européen de Recherche et

Table 2. Deep Boreholes From BEPH Database Inputted in the 3-D Middle Durance Geological Model

BEPH Boreholes	Total Depth (m)	Rock Age
Eguilles 1 (EGS1)	5385	Neogene, Paleogene, Cretaceous, and Jurassic
Grand Luberon 1 (GL1)	5042	Paleogene, Cretaceous, and Jurassic
Greoux 1 (G1)	1810	Paleogene Jurassic, Triassic, and Paleozoic
Greoux 2 (G2)	1486	Quaternary, Neogene, Jurassic, and Triassic
Greoux 3 (G3)	999	Quaternary, Paleogene, Jurassic, and Triassic
Greoux 4 (G4)	1416	Neogene Cretaceous, Jurassic, and Triassic
Greoux CD105 (GCD105)	398	Cretaceous
Jouques 1 (JQS1)	2476	Cretaceous, Jurassic, Triassic, and Paleozoic
Les Mees 1 (LM1)	1760	Neogene, Jurassic, Triassic, and Paleozoic
Manosque 1 (MA1)	1171	Paleogene (Oligocene)
Manosque 2 (MA2)	1846	Paleogene (Oligocene)
Pont-de-Mirabeau 1 (PDM1)	1799	Quaternary, Neogene, Jurassic, and Triassic
Pont-de-Mirabeau 2 (PDM2)	2073	Jurassic and Triassic
Rognes 1 (RGS1)	2369	Cretaceous and Jurassic

d'Enseignement de Géosciences de l'Environnement, and BRGM) [*Hollender et al.*, 2009]. In the present study, we gained the benefit of these previous interpretations, although we went into more detail, through the complete digitalization of the reflectors. In particular, we took care of the coherency of reflector identification at the profile crossing. These steps were performed in two-way time using the Kingdom Suite software (see IHS Kingdom services). To convert the two-way time into depth, we used the seismic stratigraphy established by the correlation of the *Grand Luberon 1* (5042 m in depth) and *Les Mées 1* (1760 m in depth) borehole stratigraphy, located in the western and eastern parts of the MDFZ, respectively, with adjacent seismic reflection lines.

A 1-D time-depth conversion law was established for these boreholes, which allowed nine stratigraphic markers to be correlated with the seismic reflectors (Figure 3) using the following velocity values: 5200 m/s for the Mesozoic, 3300 m/s for the Cenozoic on the eastern part of the MDFZ, and 2900 m/s for the Cenozoic on the western part of the MDFZ. These reflectors are (1) the base of the Valensole formation, (2) the base of the Miocene, (3) the top of the Oligocene unit (locally defined as the Montfurron limestones formation), (4) the base of the Oligocene, (5) the top of the Middle Hauterivian, (6) the top of the Middle Jurassic (locally defined as the Callovian-Oxfordian black shales), (7) the top of the Triassic (defined as the upper anhydrites), (8) the top of the Paleozoic basement (hypothesis 1) or top of the lower anhydrites (hypothesis 2), (9) the top of the Paleozoic basement (in hypothesis 2).

In the horizon-picking process, we identified two deep horizons that led to two hypotheses:

1. Hypothesis 1: the highest of both the deep reflectors is assigned to the top of the Paleozoic.
2. Hypothesis 2: the highest of both of the deep reflectors is assigned to the top of the lower anhydrites. Consequently, the lowest reflector is assigned to the top of the Paleozoic.

3.3. Cross Sections

We constructed three cross sections at the 1:50,000[e] scale, one on each of the two sides, and one across the MDF. The cross sections were also constrained by the geological maps (scale 1:50,000[e]), the outcrop dip measurements, and the depths measured in eight boreholes from the BEPH and BSS databases (Figure 5; see Figure 4 for location):

1. Section 1: This cross section is 39 km long and it crosses through the MDFZ with an E-W orientation. Section 1 comprises the Cucuron syncline and the Beaumont-de-Pertuis anticline. The depth of the Paleozoic basement ranges from 2000 to 10,000 m. This section highlights the thinning of the Middle Jurassic in the core of the footwall of the E-W orientated anticline between Grambois and Beaumont de Pertuis. This thickness variation is due to the cross-section processing, in terms of the thickness of the different stratigraphic units, their interpretation in the subsurface (with the seismic profiles), and their surface expression in the field.
2. Section 2: This cross section is 24 km long and is oriented NE-SW; it is located to the east of the MDFZ. Section 2 crosses the Greoux and Vinon-sur-Verdon thrusts and the Vautubiere anticline. Along section 2, the depth of the Paleozoic basement is around 2000 m.

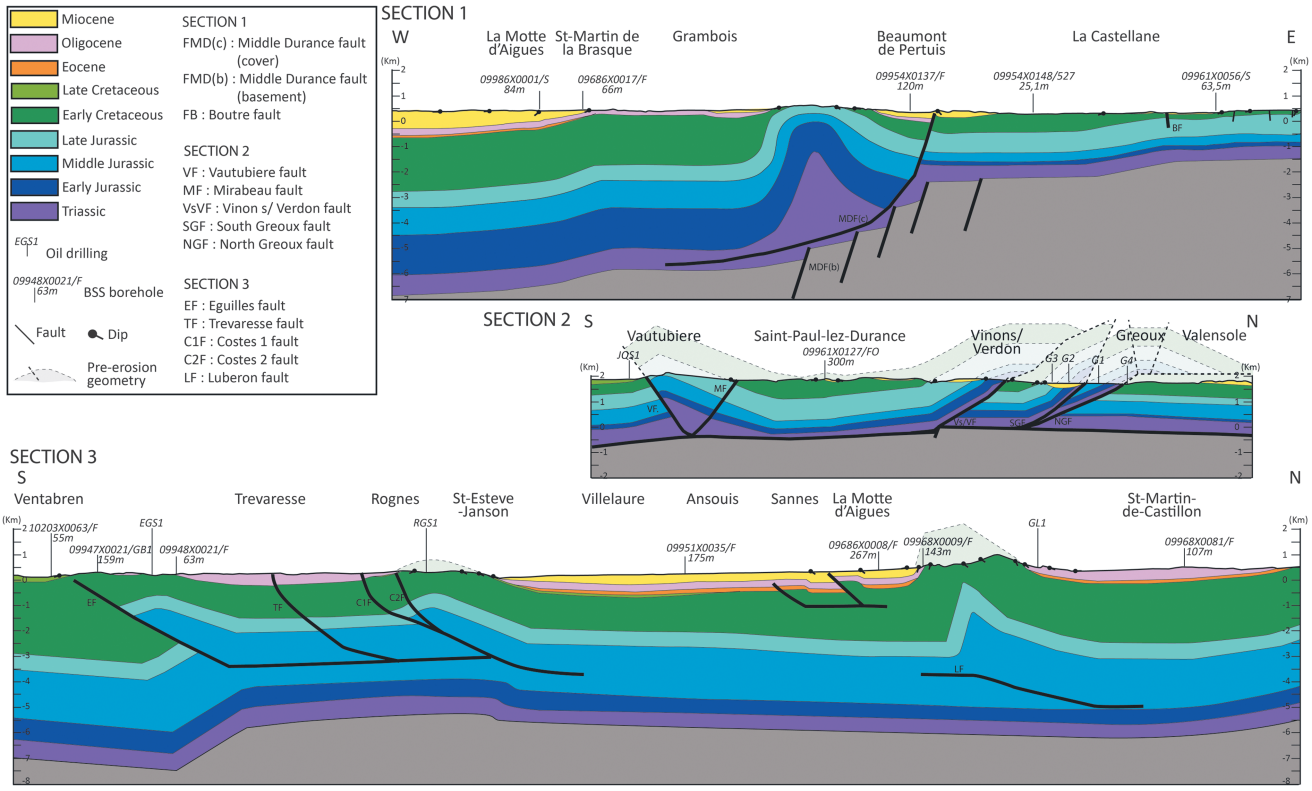

Figure 5. Middle Durance region cross sections (1 to 3). For locations, see Figure 4: red lines 1 to 3. All these cross sections cross through the entire Meso-Cenozoic sedimentary series. Section 1 crosses through the MDFZ with an E-W orientation. Section 2 is oriented NE-SW and is located to the east of the MDFZ. Section 3 is oriented NE-SW and is located to the west of the MDFZ. The legend comprises the stratigraphic units, the boreholes, and outcrops measurements represented on the cross sections. The legend also mentions the names and abbreviations of the main faults per cross section. Finally, for cross sections 2 and 3, a preerosion geometry is represented above the topography (dashed line and greyish color).

3. Section 3: This cross section is oriented NE-SW and is located to the western part of the MDFZ. It is 41 km long, and it crosses the Luberon, Coste, and Eguilles anticlines, and the Viens, Cucuron, and Trevaresse synclines. The depth of the Paleozoic basement ranges from 2000 m to 10,000 m.

These three sections cross through the whole of the Mesozoic and Cenozoic sedimentary series, except for section 2, which does not include the Oligocene unit. Three décollement levels have been interpreted from the cross sections: the Triassic evaporates, the Callovian-Oxfordian black shales, and the Valanginian marls. For example, the Vautubiere anticline and the Vinon and Greoux thrusts (Figure 5, section 2) are rooted within the Triassic evaporites at 2 km in depth. The diapiric structure between Beaumont-de-Pertuis and Grambois (Figure 5, section 1) is related to a décollement level at depths ranging from 4 km to 6 km within the Triassic evaporites. Figure 5 (section 3) reveals two décollement levels in the Callovian-Oxfordian black shales (at 3.5 km and 4.5 km in depth, for the Eguilles and Costes anticlines and the Luberon anticline, respectively), and in the Valanginian marls (at 1 km in depth beneath the Cenozoic syncline structures of the Luberon foreland, located in Sannes and La Motte d'Aigues). The occurrence of these décollement levels implies a strong genetic relationship between ramps and folds geometries. In the Middle Durance region, the ramps induce fault-bend folds and fault-propagation folds [*Suppe*, 1983].

4. The Modeling Workflow

The compilation of all of the available geophysical and geological data into a 3-D numerical model required a specific workflow within the framework of the gOcad geological software [*Mallet*, 1989, 1992, 2002; *Le Carlier de Veslud et al*., 2005; *Spottke et al*., 2005; *Caumon et al*., 2009]. The geographic reference of the 3-D structural model is the French geographic coordinate system, Lambert III. The modeling workflow was composed of three main steps [*Guyonnet-Benaize et al*., 2010] (Figure 6), described as follows.

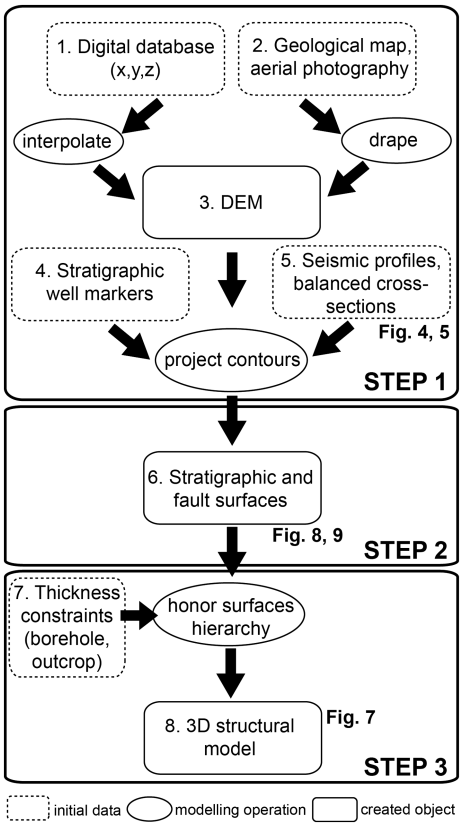

Figure 6. Modeling workflow applied for 3-D Middle Durance structural model building.

4.1. Step 1: Building the Accurate Three-Dimensional Digital Elevation Model, Including the Surface and Subsurface Data

From an IGN data set that was sampled every 25 m (Figure 6.1), we built a DEM using discrete smooth interpolator technology [*Mallet*, 1989, 1992, 2002]. The DEM obtained represents the 3-D reference surface of the model (Figure 6.2) upon which all of the data are projected or digitized. The accuracy of the DEM and of the 3-D interpreted or projected data [*Maerten et al*., 2001] depends on the accuracy of the supporting mesh [*Caumon et al*., 2009]. The aerial photographs and the geological maps were draped on the DEM as textures (Figure 6.3) to obtain a realistic 3-D image of the studied outcrop. The field data (e.g., dip and thickness measurements) and the location and depth of each borehole and its geological information (i.e., the main stratigraphic boundaries) were integrated in the geomodeler (Figure 6.4). The cross sections and the depth-converted seismic reflection profiles (Figure 6.5) were imported as vertical images. Using these images, lines of geological contacts (from cross sections) or horizons (from seismic profiles) and fault traces were digitized as points and polylines in three dimensions. The contours of each major lithostratigraphic unit were digitized and georeferenced on the IGN topographic map, at a scale of 1:25,000 [*IGN*, 1996a, 1996b, 1999, 2002] in a geographic information system. Twelve geological maps from the BRGM (scale 1:50,000) were used for the outskirts of the high-resolution geological map. The following major stratigraphic boundaries were extracted from these maps: (1) the Miocene base, (2) the Oligocene base, (3) the top of the Mesozoic, (4) the top of the upper Jurassic, (5) the top of the Middle Jurassic, and (6) the top of the Triassic. These limits and the seismic reflectors identified (see section 3.2) were imported as curves into the geomodeler.

4.2. Step 2: Building the Stratigraphic and Fault Surfaces and Respecting the Crosscutting Relationships Between the Stratigraphic and Fault Surfaces

The available surface and subsurface data were used to build the stratigraphic and fault surfaces in three dimensions with discrete smooth interpolation technology [*Mallet*, 1989] (Figure 6.6). The stratigraphic surface modeling was constrained with the stratigraphic horizons and contours digitized from maps, cross sections, seismic reflection profiles, and stratigraphic well markers. The fault surface modeling was constrained by fault traces on seismic reflection profiles, fault traces, and fault-dip angles measured in the field. The validity of a model depends mainly on the spatial distribution of the sampling relative to the variability of the surface [*Mallet*, 2002; *Caumon et al*., 2009]. The combination of measurements and interpretations allowed unrealistic fault and stratigraphic surfaces geometries to be resolved in three dimensions, due to uncertainties in each type of data and depending on the data precision and resolution. We applied thickness constraints to the interpolated horizons (Figure 6, process 7) to correct the minimal stratigraphic surface artifacts between the seismic reflection profiles and the cross-section interpretation curves. This modeling step is of paramount importance to improve the quality of the 3-D structural model and to realize realistic and accurate 3-D geometry of the stratigraphic units and faults.

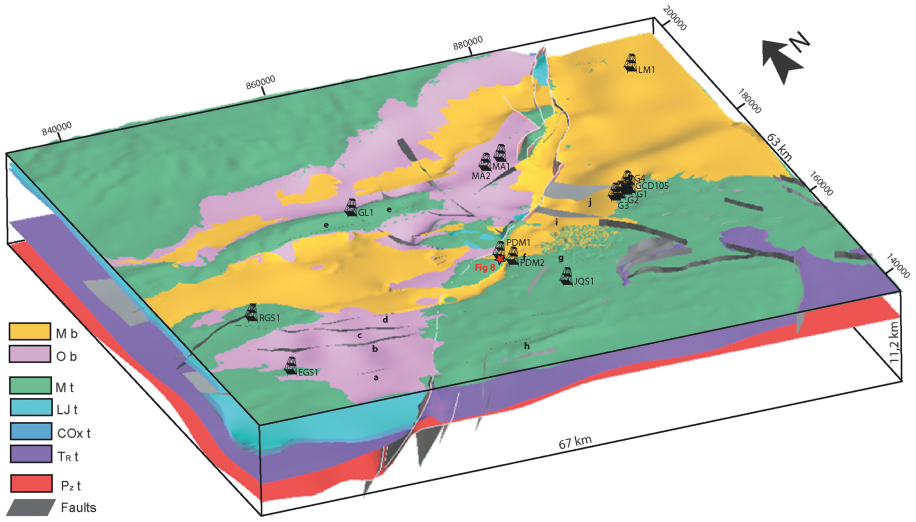

Figure 7. Three-dimensional view of the Middle Durance structural model. Major faults: (a) Eguilles, (b) Trevaresse, (c and d) Costes, (e) Luberon, (f) Mirabeau, (g) Vautubiere, (h) Sainte-Victoire, (i) Vinon, and (j) Greoux. **M b**, base of the Miocene; **O b**, base of the Oligocene; **M t**, top of the Mesozoic; **LJ t**, top of the Upper Jurassic; **COx t**, top of the Callovian-Oxfordian; **TR t**, top of the Triassic evaporates; **PZ t**, top of the Paleozoic basement.

4.3. Step 3: Geological Postprocessing of the Three-Dimensional Structural Model

In this step, we checked the chronological and geometric relationships between the stratigraphic surfaces and the fault surfaces that were established a priori in the field. In the case of the deep geometry of fault surfaces, we applied a specific workflow that depended on the fault type considered [*Mallet*, 2002; *Caumon et al.*, 2009], using different types of data, as well as single traces on seismic reflection profiles and/or on a geological cross section. We modeled normal faults from an initial vertical triangulated surface and reverse faults from an initial dipping triangulated surface. We checked the crosscutting hierarchy between the stratigraphic surfaces, between the fault surfaces and between both surfaces, which was transformed into a crosscutting hierarchical tree between all of the surfaces. Such geological postprocessing guaranties as much as possible the 3-D geological coherency of the structural model (Figure 6, process 8), despite the high heterogeneity of the input surface and subsurface set. This model is presented and interpreted below (see section 5, section 6).

5. Results: The Three-Dimensional Structural Model of the Middle Durance Fault Zone

The 3-D structural model of the MDFZ is illustrated in Figure 7. This 3-D model covers an area of 67 km × 63 km, down to a depth of 11.2 km. Figure 7 shows the complex present-day geometry of the structural and stratigraphic architecture, with 46 faults and the seven stratigraphic surfaces of the base Miocene, the base Oligocene, the top of the Mesozoic, the top of the upper Jurassic, the top of the Callovian-Oxfordian, the top of the Triassic evaporites, and the top of the Paleozoic basement.

The 3-D model shows two major unconformities: the base of the Oligocene (Figure 8, pink) and the base of the Miocene (Figure 8, yellow). These angular unconformities are observed in the field (Figure 8, lying unconformably on Cretaceous limestones) and in the seismic reflection sections [*Hollender et al.*, 2009]. The faults characterized by a throw that is smaller than the resolution of the 3-D grid (cell size: 10 m × 10 m × 2 m) have been removed, leaving only the 46 faults plurikilometer scale. These faults are characterized by variable strikes: 16 faults trend NE-SW, 16 faults trend E-W, 9 faults trend NW-SE, and 5 faults trend N-S. The 3-D model allows the distinction between two families of faults, as 23 major faults and 23 minor faults, on the basis of multiple criteria (e.g., surface trace, length, throw, strike, and dip). The major faults are the Eguilles, Trevaresse, Costes, and Luberon faults to the west (Figure 7, faults a–e), and the Mirabeau/Vautubiere, Sainte-Victoire, Vinon, and Greoux faults to the east (Figure 7, faults f–j). The patterns of the major faults are dominated by listric

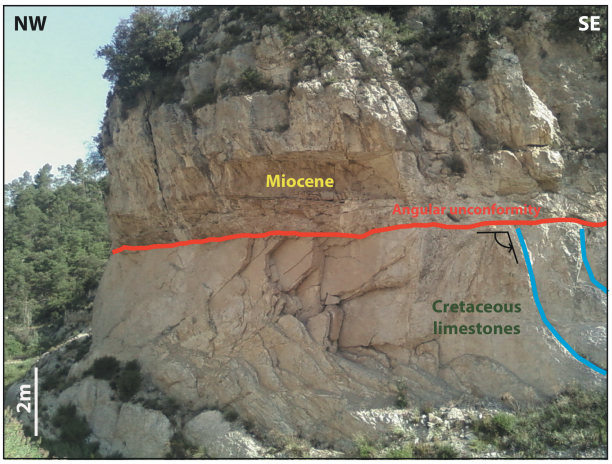

Figure 8. Angular unconformity between the Miocene and Cretaceous rock. Photograph showing the Miocene calcarenites lying unconformably on Cretaceous limestones.

geometries with reverse movement, except for three faults that show vertical geometry and normal displacement. These major faults divide the study area into two homogeneous structural blocks: a western block and an eastern block, separated by the MDFZ.

5.1. The Paleozoic Basement

The top of the Paleozoic basement forms the base surface of the 3-D structural model and controls the sharp variations of thickness of Meso-Cenozoic cover (Figure 9a). To the east, the average altitude is −2250 m above mean sea level (amsl), which ranges from −1000 m to −3500 m amsl. The surface morphology is flat, with a slight N-S altitude gradient. To the west, the average altitude is −8000 m amsl and this ranges from −6000 m to −10,000 m amsl, with a flat morphology. The transition zone between these two areas is affected by eight normal faults, with a staircase step geometry (Figure 9a) that corresponds to the deep part of the MDFZ.

5.2. The Mesozoic Series

Figure 9b shows the present-day altitude geometry of the top surface of the Mesozoic series. The mean altitude of this surface over the study area is close to −250 m amsl, with a range from 1000 m to −1500 m amsl. The Mesozoic thickness increases toward the north-west, to 1750 m and 8750 m on average, to the east and the west of the MDFZ, respectively (Figure 9c and Table 3). The top of the Mesozoic surface 3-D geometry is characterized by structural highs that strike E-W and NW-SE, which correspond to anticline axes to the east and west of the MDFZ, respectively, which are separated by synclines (i.e., Tertiary erosional surfaces) that range from −500 m to −1000 m amsl (Figure 9c). Within the synclines, the strata are characterized by asymmetric and wedging geometries, with variations in the bedding thickness. To the east of the MDFZ, the anticlines are the Vinon-Greoux, Vautubière/Mont Major, and Sainte-Victoire structures (Figure 9b) and these reach 600 m to 1000 m amsl. These structures have a Mesozoic thickness that ranges from 2000 m to 4000 m (Figure 9c). For the synclines, the Mesozoic thickness ranges from 6500 m to 7000 m on average, except for the Valensole basin, where the Mesozoic deposits are only 500 m to 1000 m thick. To the west of the MDFZ, the anticlines are the Monts de Vaucluse, Luberon, and Costes structures (Figure 9b), and these reach 400 m to 1000 m amsl. These structures have a Mesozoic thickness that ranges from 8500 m to 10,000 m (Figure 9c). For the synclines (Manosque-Forcalquier, Cucuron, and Aix-en-Provence), the Mesozoic thickness ranges from 6200 m to 7600 m on average, except for the Manosque-Forcalquier basin, where the Mesozoic deposits are only 4000 m thick.

5.3. The Cenozoic Cover

The Tertiary surfaces, as the base of the Miocene (Figure 10a) and the base of the Oligocene (Figure 10b), cut through the top of the Mesozoic surface. The base of the Miocene surface is preserved in present-day topographic depressions, as inherited from Mesozoic synclines to the west of the MDFZ (Manosque-Forcalquier, Viens, and Cucuron) and to the east of the MDFZ (Valensole) and in the present-day Durance valley (Peyrolles and Pont-de-Mirabeau). The base of the Miocene reaches an altitude of −300 m and 250 m amsl on average, to the east and the west of the MDFZ, respectively (Table 3). The base of the Oligocene surface is only located to the west of the MDFZ, and this comprises several depressions that correspond to the present-day basins of Manosque-Forcalquier, Viens, and Cucuron. The base of the Oligocene surface reaches an altitude of −600 m amsl on average (Table 3), where its maximum depth corresponds to the Manosque-Forcalquier basin.

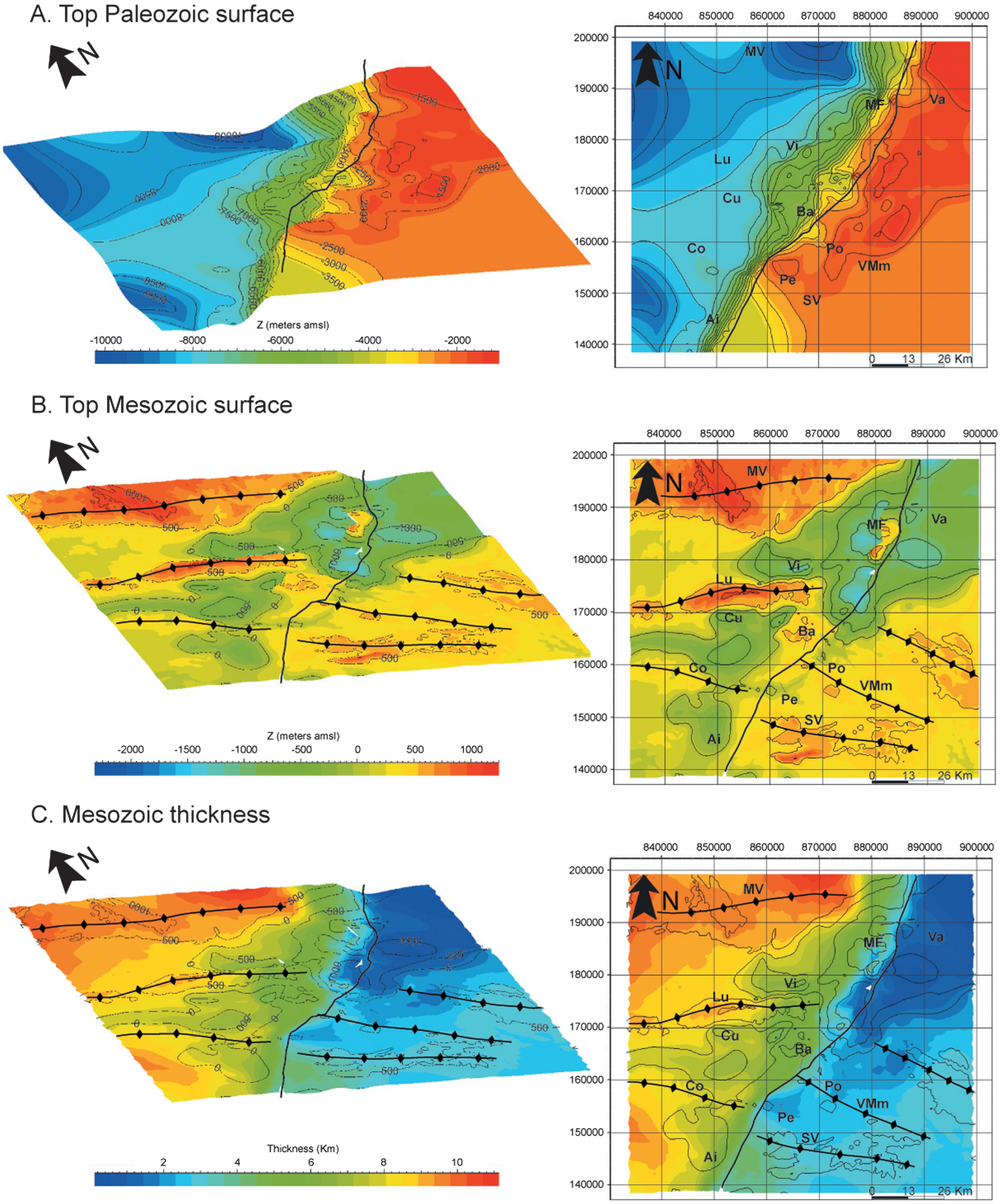

Figure 9. (left) Three-dimensional and (right) map views of the top of the (a) Paleozoic basement, (b) the top of the Mesozoic surface, and the (c) Mesozoic thickness, projected on the top of the Mesozoic surface (Figure 9b). Anticline axes are represented by black lines with diamonds. Contour lines in grey, in each panel are the elevation contours (in meters, amsl). Ai, Aix-en-Provence; Ba, la Bastidonne; Co, Costes; Cu, Cucuron; Lu, Luberon; MF, Manosque-Forcalquier; MV, Monts de Vaucluse; Pe, Peyrolles; Po, Pont-de-Mirabeau; SV, Sainte-Victoire; Va, Valensole; Vi, Viens; and VMm, Vautubiere/Mont Major.

Table 3. Mean Depth of the Paleozoic Basement, Top Mesozoic, and Cenozoic (Oligocene and Miocene Bases) 3-D Surfaces[a]

3-D surfaces	Location	Mean depth (m)	Depth Min	Depth Max
Miocene base	West of MDFZ	250	−200	700
	East of MDFZ	−300	−1200	600
Oligocene base	West of MDFZ	−600	−1400	200
Top Mesozoic		−250	−1500	1000
Paleozoic basement	West of MDFZ	−8000	−6000	−10000
	East of MDFZ	−2250	−3500	−1000
Stratigraphic units	Location	Mean Thickness (m)	Thickness Min	Thickness Max
Cenozoic	West of MDFZ	850	500	1200
	East of MDFZ	1250	500	2000
Mesozoic	West of MDFZ	8750	6500	11000
	East of MDFZ	1750	500	3000

[a]Mean thickness of Mesozoic and Cenozoic sedimentary series.

Figure 10c shows the Tertiary thickness. We only calculated the thicknesses of the Oligocene and Miocene units, as the Eocene deposits are not significant in the study area, with a thickness $\leq$60 m. The Cenozoic thickness reaches 1250 and 850 m on average, to the east and the west of the MDFZ, respectively (Table 3). Throughout the study area, the altitude of both of the surfaces (Figures 10a and 10b) reveals two major depressions: Manosque-Forcalquier to the west and Valensole [*Ford et al*., 1999] to the east. The altitudes of these depressions are −1400 m and −1000 m amsl, respectively, with an average thickness of the tertiary sediments to 1500 m and 300 m, respectively (Figure 10c). To the east of the MDFZ, the deposits are Miocene to Pliocene in age, with Oligocene deposits being absent (except from the lacustrine limestone of Montmeyan). Therefore, the base of the Oligocene surface is not modeled to the east of the MDFZ. The deposits that fill this depression are detrital (mainly conglomerates) and these result from erosion of the Alps [*Dubar*, 1983; *Dubar et al*., 1998]. To the west of the MDFZ, in the depression of Manosque-Forcalquier, the difference of altitude between Miocene (+200 m amsl) and Oligocene (−1400 m amsl) base surfaces is nearly 1600 m.

5.4. The Fault Pattern

The 3-D fault network characterization leads us to propose a new detailed segmentation of the associated structures of the MDFZ (Figure 11). In the following description, we use a "structural segmentation" terminology, with no correlation to the "seismic segmentation" terminology relating to the breaking up of a fault along its length.

West of the MDFZ, there are 12 faults (faults 1–12). Among these faults, seven faults correspond to thrust faults (faults 1–4 and 7–9), four faults can be seen at the surface (faults 5, 6, 8, and 9), five cannot be seen at the surface (faults 1, 7, and 10–12), and finally, three can be seen in part at the surface and have been modeled in depth (faults 2–4). East of the MDFZ, there are eight faults that correspond to thrust faults (faults 13–20). Here four faults can be seen at the surface (faults 13–15 and 19), one fault is not seen at the surface (fault 17), while three faults can be seen in part at the surface and have been modeled in depth (faults 16, 18, and 20).

6. Interpretations

6.1. Vertical and Horizontal Segmentation of the Middle Durance Fault Zone

The MDFZ has been defined as a fault network that extends down to 6 km in depth [*Terrier*, 1991; *Cushing and Bellier*, 2003; *Cushing et al*., 2008; *Molliex*, 2009], which has been based on mapping (i.e., fault traces on the surface), seismogenic, geomorphological, and geophysical criteria (i.e., seismic reflection sections). Our 3-D model allows further interpretation and defines a fault network geometry that extends down beyond 6 km and reaches 12 km in depth.

In the subsurface, the MDFZ has a variable and complex geometry (Figure 12), and thus it can be qualified as a "fault zone." It is divided into two levels, as follows. The deeper of these two levels is composed of eight fault segments that are interpreted from seismic reflection profiles as normal faults that affect the Paleozoic basement (Figure 12a). These faults are orientated N030° to N040°, and they have dip that varies from 55° to 64° to the west. These provide the staircase geometry (i.e., a normal faulting system) of the basement, and they correspond to the southeastern boundary of the SE Basin at the regional scale. The second of these two levels is a shallow level, and it is composed of seven segments (Figure 12b).

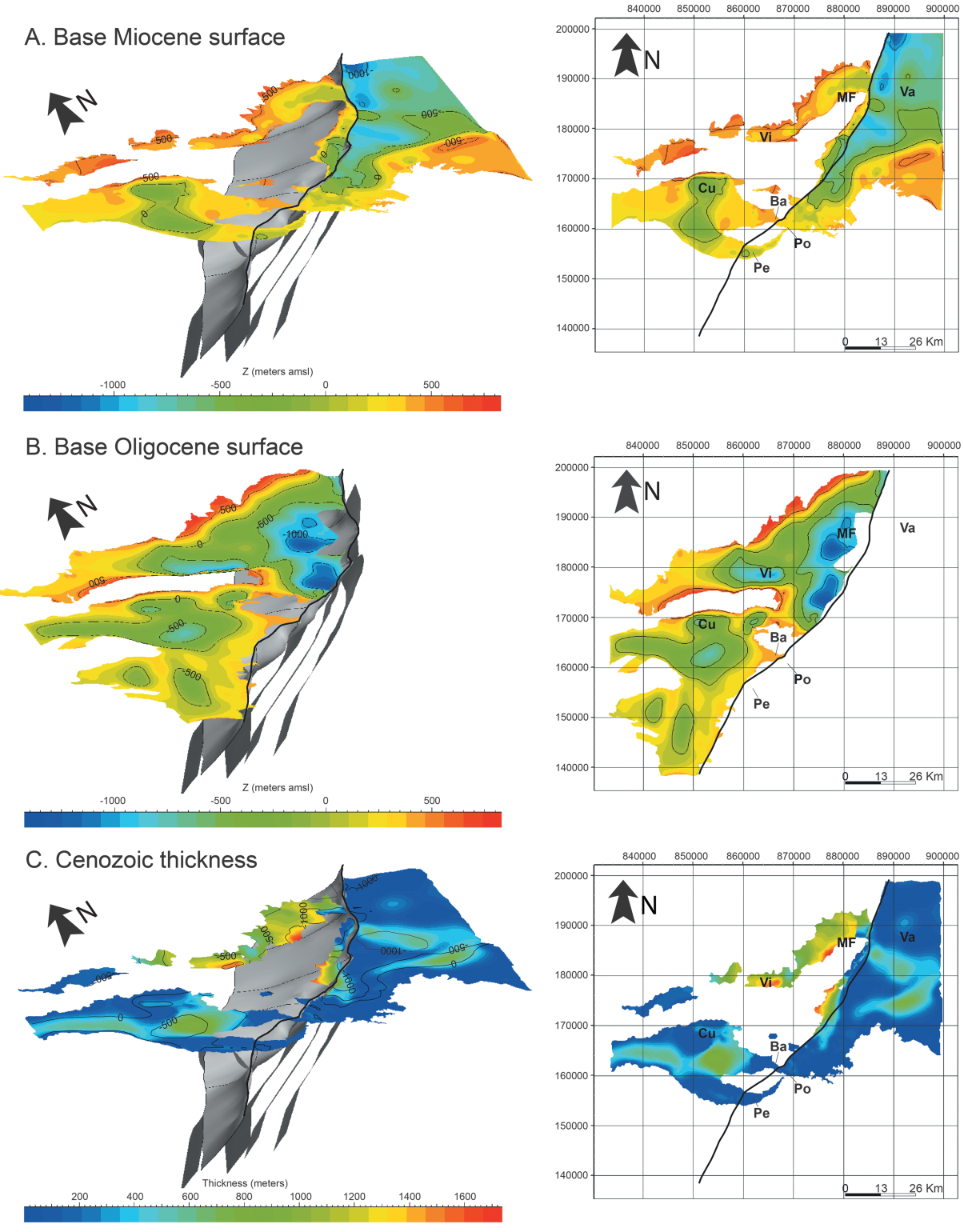

Figure 10. (left) Three-dimensional and (right) map views of (a) the base of the Miocene surface, (b) the base of the Oligocene surface, and (c) the Cenozoic thickness, projected on the top Miocene surface (Figure 10a). Contour lines in grey, in each panel are the elevation contours (in meters, amsl). Ba, la Bastidonne; Cu, Cucuron; MF, Manosque-Forcalquier; Pe, Peyrolles; Po, Pont-de-Mirabeau; Va, Valensole; and Vi, Viens.

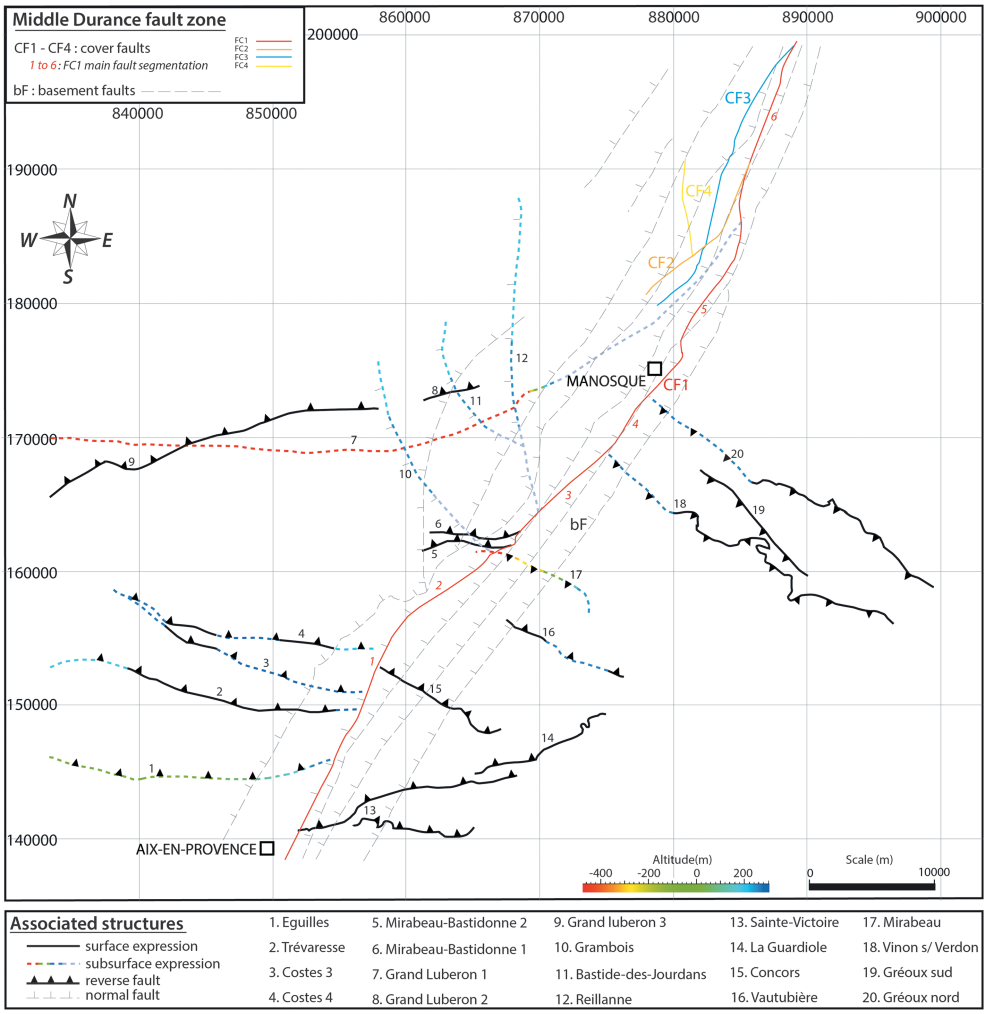

Figure 11. New 3-D segmentation of the Middle Durance Fault Zone and its associated tectonic structures. The associated tectonic structures are in black and colored dashed lines; MDFZ with cover faults CF1 to CF4 are in colored lines, and basement faults are in black thin dashed lines.

The main shallow fault (CF1) is composed of five relay fault segments [*Terrier*, 2004a, 2004b] that strike N025°. These faults have a listric geometry with reverse movement, and they are rooted in the Triassic evaporitic layers between 2000 and 4000 m in depth. The two faults CF2 and CF3 strike N021° to N025° (Figure 12c) and they have listric geometry with reverse movement, and are connected to CF1 at depth. They have a normal throw (900 m) and affect the entire Mesozoic series. The fault CF4 is N175° striking, and it is conjugated to CF1 and has a 45° dip toward the east. The faults CF2 to CF4 (Figure 12d) were constrained with seismic and outcrop data, and they explain the presence of Cretaceous rock at the surface in this area. Figure 12e shows the depth of the top Mesozoic surface. This surface is 600 m high between CF2 to CF4 and the CF1 fault, while reaching a depth of 1500 m to the west of these faults. These segments were identified and modeled from seismic data and fault traces on the surface [*Cushing and Bellier*, 2003], and they affect the Mesozoic to Cenozoic sedimentary cover (Figure 12d).

There is no apparent connection between these faults of the deep and shallow levels of the MDFZ. The shallow faults of the MDFZ are located below the deeper normal faults of the MDFZ, but no sedimentary cover fault extends into the Paleozoic basement, and vice versa. The main MDFZ shallow fault (CF1) is rooted in the Triassic evaporitic layers, above the Paleozoic basement. The shallow faults above (CF2 to CF4) affect only the Meso-Cenozoic deposits. Moreover, the microseismic activity recorded in this area has been located to the Meso-Cenozoic sedimentary cover [*Lin and Le Pichon*, 2007; *Cushing et al.*, 2008]. We can

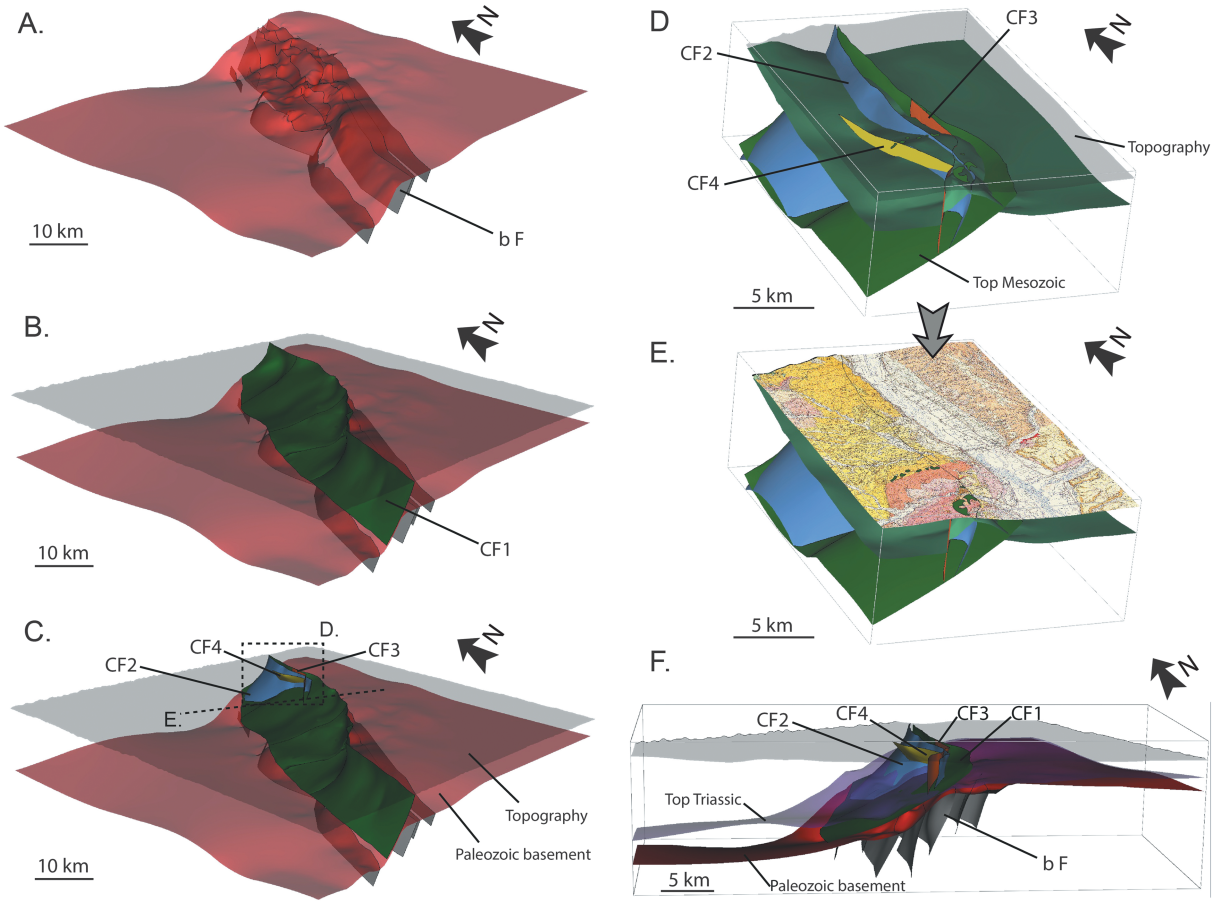

Figure 12. Three-dimensional present-day geometry of the Middle Durance Fault Zone. (a) Faults affecting the Paleozoic basement (b F). (b and c) Faults (CF1–CF4) affecting the Mesozoic to Cenozoic cover. (d) Expanded from box D in Figure 12c, showing the geometry of faults CF2 to CF4 and the (e) observed Cretaceous rock at the surface. (f) Three-dimensional cross section showing the MDFZ 3-D geometry: listric segmented faults (CF1 to CF4) anchored in the Triassic layers and normal faults in the Paleozoic basement (b F).

conclude that the shallow fault system of the MDFZ is an active fault system that reaches the Triassic evaporitic layers, and that the deeper fault system remains inactive.

This 3-D geometry of the MDFZ shows that the fault cannot be interpreted as a single fault plane that affects the entire Mesozoic series and the Paleozoic basement. On the contrary, the MDFZ is composed of listric segmented faults in the Mesozoic cover that are rooted in the Triassic layers and normal block faults in the Paleozoic basement, with the decoupling level in the Triassic layers (Figure 12f).

6.2. The Three-Dimensional Fold Geometry

The main tectonic structures observed in the field are anticlines that affect Jurassic to Cretaceous rock. These folds are the result of the process of thin-skin deformation that affects the eastern and western parts of the MDFZ. The deformation that affects the Middle Durance region has been modeled with three main décollement levels in the Mesozoic sedimentary cover, the deeper one being rooted in the Triassic evaporites, at the Mesozoic base. These décollement levels show the thin-skin deformation, which is characterized by listric faults that are anchored in the Triassic evaporitic layers. The maximum normal throw on the MDFZ, calculated using the top of the Paleozoic basement throw, reaches 5600 m.

To the west of the MDFZ, the main folds are the Grand Luberon anticline and the Costes and Eguilles thrusts, which are separated by structural flats and characterized by a length of 5 km to 6 km. The Grand Luberon anticline is a south-verging asymmetric ramp-fold, which strikes E-W with a 70° to 80° dipping south flank and a 30° to 50° dipping north flank. The Luberon fold developed above the upward propagating listric faults in

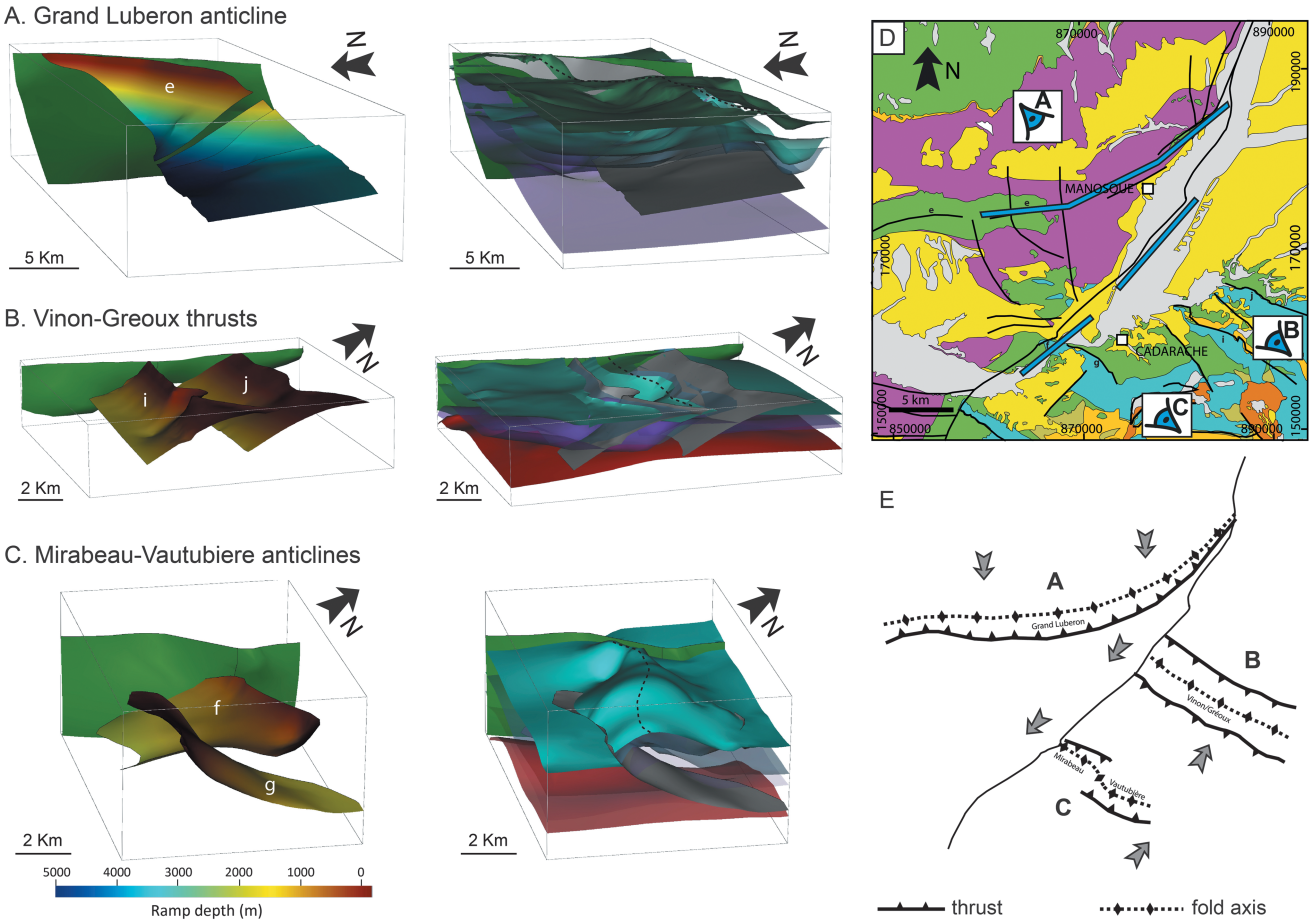

Figure 13. Various fold geometries of the Middle Durance region. (left) Three-dimensional views of the ramp depths and for the (middle) folds above the ramps for the (a) Grand Luberon anticline, (b) Vinon-Greoux thrusts, and (c) Mirabeau-Vautubiere anticlines in the western and eastern parts of the MDFZ, respectively. (d) Locations of the 3-D views of the ramps and folds shown in Figures 13a–13c. (e) Conceptual sketch showing the geometrical relations between the ramps, folds, and the MDFZ. Major faults: Trevaresse (b), Costes (c, d), Luberon (e), Mirabeau (f), Vautubiere (g), Vinon (i), and Greoux (j).

the Mesozoic sedimentary cover, which are rooted in the Callovian-Oxfordian black shales (Figure 5, section 3 and Figure 13a). We interpret the Grand Luberon anticline as a fault-propagation fold, based on the asymmetrical shape of this fold and the high-dipping values of its southern flank. The Costes and Eguilles thrusts are south-verging E-W-striking ramp anticlines. These thrusts are characterized by a symmetric geometry with equal dips on both flanks (25° for Costes thrust, 20° for Eguilles thrust). We interpret the Costes and Eguilles thrusts as fault-bend folds. East of the MDFZ, the main tectonic structures are the Vinon-Gréoux, Guardiole, Sainte-Victoire, and Vautubière/Mirabeau thrusts and the Concors anticline. These structures are either south-verging (Sainte-Victoire, Guardiole, and Concors) or north-verging (Vinon-Gréoux) ramp folds that strike NW-SE. These folds have a length of 2.5 km to 3 km and have symmetric geometry with equal dip values on both flanks (e.g., 40° for Vinon-Gréoux thrust, Figure 5, section 2; Figure 13b). We interpret these thrusts and anticlines as fault-bend folds. The Mirabeau and Vautubière anticlines form an asymmetric fold with double vergency thrust ramps (north vergency for the Mirabeau fold, south vergency for the Vautubière fold; Figure 13c). We interpret these two folds as fault-propagation folds that are linked by a transfer zone, which corresponds to an antithetic thrust fault [*Higgins et al*., 2007]. Figure 13c shows the switch in the vergency of the folds along the strike, which corresponds to an antithetic thrust fault linkage below. The shapes and sizes of the folds allow the calculation of the depth of their décollement level [*Higgins et al*., 2007]. The interpretation of the seismic reflection profiles and the cross sections supports the identification and modeling in three dimensions of three main décollement levels in the Triassic evaporitic layers, in the Callovian-Oxfordian black shales, and in the Valanginian marls. West of the MDFZ, the ramp folds have two décollement levels. The lower level is located in the Callovian-Oxfordian black shales, from 3500 to 4000 m

deep. This level is relayed to an upper level in the Valanginian marls, at 1000 m in depth. East of the MDFZ, the ramps are rooted in a single décollement level in the Triassic evaporitic layers, from 1700 to 1800 m in depth.

We can conclude that the main Middle Durance tectonic structures are fault-bend folds and fault-propagation folds that have resulted from folding of the Mesozoic sedimentary series. The 3-D model shows the two main controlling factors of the fault-bend and fault-propagation folds, on each side of the MDFZ: (1) the thickness of the sedimentary cover above the Paleozoic basement (2 km to the east, 10 km to the west) and (2) the presence of three décollement levels in the sedimentary cover that is located in the Triassic, Callovian-Oxfordian, and Valanginian units (dominated by marls or evaporites). The strong variations in both the sediment thickness and the décollement depth explain the lack of fold continuity on each side of the MDFZ.

6.3. The Role of the Middle Durance Fault Zone on the Geometry of the Tectonic Structure

Variable fold geometries have been illustrated between the western (Grand Luberon anticline) and eastern (Vinon-Greoux thrusts and Mirabeau-Vautubiere anticlines) parts of the MDFZ (Figure 13). The 3-D views of ramp depths (Figure 13, left) show that the Vinon-Greoux and Mirabeau-Vautubiere anticlines (Figures 13b and 13c) have ramps that are rooted at 2 km deep, and the Grand Luberon anticline (Figure 13a) has a ramp that is rooted at 5 km deep. The 3-D views in the middle of Figure 13 show the 3-D geometry of three folds above the ramps. These folds are all linked to the MDFZ and especially to the main segment (CF1). The geometric relationships between these folds and the MDFZ can be split into three types as follows.

1. "Drag fold," as for the Grand Luberon fold (Figure 13a). At the surface, this fold has a fold axis striking E-W (in the Luberon area), then NE-SW (in the Manosque area) close to the MDFZ. In the subsurface, the fold ramp is rectilinear, striking E-W and with roots that are 5 km deep (in the Luberon area) in the Callovian-Oxfordian black shales. The ramp is curved (in the Manosque area) close to the MDFZ, striking NE-SW.
2. "Rectilinear axis" fold, as for the Vinon-Greoux fold (Figure 13b). At the surface, this fold has a symmetrical geometry and strikes NW-SE. The axis of this fold is rectilinear and perpendicular to the MDFZ. In the subsurface, the fold has two ramps with south vergency. These ramps are rooted 1.5 km deep. The fold has asymmetrical shape geometry, with a high-dipping south flank.
3. "En echelon" fold, as for the Mirabeau-Vautubiere fold (Figure 13c). At the surface, this fold has a symmetrical geometry and strikes NW-SE. The axis of this fold is rectilinear and perpendicular to the MDFZ. In the subsurface, the fold has two ramps with opposite vergency: a north vergency ramp (Mirabeau), and a south vergency ramp (Vautubiere). These ramps are rooted 2 km deep in the Triassic evaporites. The 3-D view of the Mirabeau-Vautubiere fold reveals an asymmetric shape of this fold between the two ramps. The Mirabeau-Vautubiere fold can be considered as an antithetic thrust fault linkage [*Higgins et al*., 2007].

These three examples show that the geometry of the folds is modified close to the MDFZ, in a band of 8 km, apart from the main fault segment (CF1). From these observations, we can argue that the MDFZ is a transfer fault.

7. Discussions

7.1. Deformation Style

The geological structure of the Provence area, and more precisely the Middle Durance area, has traditionally been interpreted using thin-skinned thrust tectonic models, in which the Meso-Cenozoic sedimentary cover has been detached from the Paleozoic basement below. Such models have been used to estimate the crustal shortening, and especially the Miocene shortening [*Champion et al*., 2000; *Molliex et al*., 2011], in this region. In the present study, we have reinterpret the deformation style of the Middle Durance region with our integrated approach that is based on 3-D modeling, and we have discussed the thin-skin deformation hypothesis. Many studies based on a seismic, seismo-tectonic, or field approach have demonstrated the existence of an extensional tectonic regime with décollement of the Mesozoic cover during the Oligocene rifting in the Manosque basin [*Roure et al*., 1992; *Benedicto Esteban*, 1996]. To the west of the MDFZ, the sedimentary cover accommodates a part of the thin-skin deformation by sliding on the Paleozoic basement [*Baroux*, 2000]. Our study has demonstrated the mechanical decoupling between the Mesozoic cover and the Paleozoic basement, linked to the Triassic evaporitic layers. These layers correspond to an incompetent ductile level that allows the disharmonic deformation geometries observed. For the E-W folds, the cross

sections and the borehole data enabled the modeling of thrust-rooted ramps in such a ductile décollement level, as well as the rooting of the fault plan of the MDFZ. The deformation of the Meso-Cenozoic sedimentary cover is accommodated along the MDFZ, through the Triassic evaporates for both parts of the MDFZ and also through higher levels in the sedimentary cover, e.g., the Callovian-Oxfordian black shales and the Valanginian marls on the western part of the MDFZ.

Many studies have indicated that the deformation above the décollement levels has been active, at different times during the history of the Meso-Cenozoic basin. *Roure et al*. [1992] indicated the difference between the rate of pre-Oligocene (3%) and Oligocene (15%) extensions, as calculated in the Mesozoic sedimentary cover. This difference is interpreted as an important "slope" to the west of the Mesozoic sedimentary cover on the Paleozoic basement during the Oligocene extension, without intra-Paleozoic deformation. *Benedicto Esteban* [1996] and *Champion* [1999] suggested that the deformation would thus be limited to the sedimentary cover, based on seismo-tectonic criteria.

For the role of the MDFZ in such observed deformations, *Benedicto Esteban* [1996] and *Champion* [1999] made the assumption that the MDFZ has acted as an active lateral ramp since the Mesozoic times, to separate the autochthonous series to the east and the allochthonous series to the west. In contrast, another study suggested the involvement of basement faults in the regional deformation [*Sébrier et al*., 2004]. However, earthquake nucleation to the west of the MDFZ [*Le Pichon et al*., 2010] allowed the observation that the active seismicity is located at a depth of less than 4 km to 5 km in the Mesozoic cover. For *Le Pichon et al*. [2010], earthquake production was probably caused by cover faults or gravity slope on the Triassic evaporitic layers. The MDFZ microseismic activity, which is essentially located in sedimentary cover, suggests strong mechanical decoupling between the basement and the cover [*Baroux*, 2000; *Bellier et al*., 2007]. Indeed, *Baroux* [2000] and *Bellier et al*. [2007] reported that the seismic activity occurs only in the Mesozoic and Cenozoic sedimentary cover, with most of the earthquakes located above the Paleozoic basement.

In the literature, the MDFZ has been described as a normal fault during the Mesozoic times [*Baudrimont and Dubois*, 1977; *Roure et al*., 1992; *Benedicto Esteban*, 1996; *Cushing et al*., 2008]. This is illustrated in our 3-D model, with the increasing thickness of the Mesozoic series from the MDFZ to the western part of the basin (see Figure 9c). During the Pyrenean compression (Upper Cretaceous to Paleogene) [*Benedicto Esteban*, 1996; *Roure and Colletta*, 1996; *Cushing et al*., 2008], the MDFZ acted as a reverse and strike-slip faulting system. As in the literature, our model shows (see section 7.1) that the fault and thrust folds caused by the Pyrenean compression have modified 3-D geometries close to the MDFZ, which reveals that the MDFZ is a transfer fault at this time. Studies have described the MDFZ as a normal fault during the Oligocene age [*Benedicto Esteban*, 1996; *Roure and Colletta*, 1996; *Cushing et al*., 2008; *Hollender et al*., 2009]. Our model shows that Oligocene deposits are located in depressions in the western part of the MDFZ and that their extension is limited to the east by the MDFZ. These observations confirm the normal faulting activity of the MDFZ sedimentary cover faults during the Oligocene times.

In conclusion, the results of our 3-D structural model are consistent with previous studies. Mesozoic and Cenozoic thickness maps and the 3-D geometry of folds and faults confirmed from previous studies illustrate the tectonic activity of the MDFZ during the Mesozoic and Cenozoic times. Earlier studies based on fewer geometric arguments are strengthened by our model, which provides a constrained 3-D geometry. It can be concluded that the Middle Durance region is characterized by a thin-skin deformation that occurs through strong mechanical decoupling between the Mesozoic sedimentary cover and the Paleozoic basement.

7.2. Synsedimentary Tectonics and Structural Inheritance During the Mesozoic

We have shown that the MDFZ had a complex 3-D geometry that was characterized by normal faults in the Paleozoic basement and listric faults in the Mesozoic cover. The decoupling level locates to the Triassic evaporitic layers. We have also shown that the 3-D geometry and the termination of the folds were modified near the MDFZ. Taking into account that from most studies the MDFZ microseismic activity is essentially located in the Mesozoic sedimentary cover [*Chardon and Bellier*, 2003; *Guignard et al*., 2005; *Le Pichon et al*., 2010], it can be asked whether the recent tectonic activity of the MDFZ was associated to a strike-slip fault that involved the Paleozoic basement or to a transfer fault that was limited to the Mesozoic cover.

Previous studies have considered the MDFZ as a strike-slip fault that was inherited from late Hercynian deformation [*Debrand-Passard et al*., 1984], because of the heterogeneous geometries of the Mesozoic series.

Other studies have suggested that the major E-W folds (i.e., Luberon and Mont Ventoux) might have been initiated by the MDFZ acting as a reverse fault since the Pyrenean age [*Clauzon*, 1984; *Villegier and Andrieux*, 1987]. These have shown deformation that affects the Tortonian deposits (Middle Miocene) in the foreland of the E-W oriented Grand Luberon anticline, which highlights the late reactivation of this structure as thrust. Deformation observed along the MDFZ would be due to the transfer of the stress from the Alps toward the foreland [*Baroux*, 2000]. In other studies, the MDFZ has been indicated as a Paleozoic basement seated fault during the Oligocene times [*Biondi et al*., 1992]. Due to our 3-D structural model of the Middle Durance region, we can argue that the MDFZ is a transfer fault with folds and thrust that are limited by the fault, and where its influence extends primarily to the west, 7 km to 8 km from the main MDFZ segment (CF1). This transfer fault modifies the fold geometry into the drag, en *échelon* or rectilinear axis folds. Its lateral influence extends over 7 km to 8 km from the fault (Figure 13, CF1). In addition, the MDFZ separates two structural blocks with variations in the Mesozoic sedimentary series thickness. The reinterpretation of the seismic profiles and their consistency in three dimensions has allowed us to estimate the Mesozoic thickness to 11 km west of the MDFZ (as indicated by *Baudrimont and Dubois* [1977]) and to 1.5 km to 2.5 km east of the MDFZ. We have shown that the shortening linked to the Pyrenean compression induced different deformation styles on the sedimentary series that depended on the sedimentary thickness to the west and east of the MDFZ. Indeed, west of the MDFZ, the folds have both fault-propagation (i.e., Grand Luberon anticline) and fault-bend (i.e., Costes and Eguilles thrusts) folds geometries, with south vergency and steep flanks. The fold décollement level is located in the Callovian-Oxfordian black shales and/ or the Triassic evaporitic layers (i.e., Grand Luberon anticline). To the east of the MDFZ, the folds and thrusts have fault-bend fold geometry with north (i.e., Vinon-Gréoux duplex) or south (i.e., Vautubière anticline) vergency and décollement level in the Triassic evaporitic layers. For the Tertiary basin structural inheritance, we have shown that each of the main Tertiary sedimentary basins (i.e., Viens, Manosque-Forcalquier, Cucuron, and Aix basins to the west of the MDFZ; Valensole basin to the east of the MDFZ) is located between two Pyrenean E-W folds (e.g., the Cucuron basin is located between the Luberon and Costes folds). This shows that all of the Tertiary sediments are best located in depressions created between the Pyrenean tectonic structures. Most of these Tertiary basins are filled by Eocene and Oligocene deposits which demonstrate that these basins were filled by sediments before the Alpine shortening, in depressions between the Pyrenean structures. This confirms that these basins have Pyrenean structural inheritance.

7.3. Durancian Inheritance and Alpine Partitioning

In the present study, we have confirmed that the Middle Durance region has undergone successive extensional, compressional, and/or transpressional deformation steps (Pyrenean and Alpine inversions). Therefore, the present-day tectonic structures result from cumulative effects of the strain history. What is the deformation part that resulted from each deformation step? Many studies have focused on the quantification of the deformations due to the Alpine and Pyrenean orogenesis.

In Provence, *Champion et al*. [2000] suggested that the deformation mostly occurred during the Miocene and has decreased since that time. Several studies have attributed the fold setting to the Late Cretaceous [*Corroy et al*., 1964; *Leleu*, 2005], and the north-verging thrust to the Eocene [*Bertrand*, 1899; *Haug*, 1925; *Guieu*, 1968; *Tempier*, 1987]. Some studies have indicated south-verging thrust reactivation (i.e., Luberon, Costes, and Eguilles) that was related to the Alpine deformation spread [*Clauzon*, 1984; *Villegier and Andrieux*, 1987; *Blès and Gros*, 1991; *Clauzon et al*., 2011; *Molliex et al*., 2011].

In the Middle Durance region, the 3-D model that we have constructed shows that the main tectonic structures (i.e., E-W folds, thrusts) are partly inherited from a Durancian deformation and were mainly reactivated during the Pyrenean deformation. The Alpine deformation weakly reactivated these structures. Balanced cross sections have allowed the estimation of the Pyrenean and the Alpine parts of the deformation in the fold structures (e.g., the Grand Luberon anticline) [*Molliex et al*., 2011; *Lamarche et al*., 2012; *Tassy*, 2012; *Gisquet et al*., 2013; *Lavenu et al*., 2013]. We can access the structure of the post-Pyrenean and pre-Alpine folds by back tilting the Miocene marine deposits to their original flat position. Cross section 3 (see Figure 5) allows the quantification of the Miocene deformation. On this cross section on the eastern part of the Luberon anticline, the Miocene shortening is 550 m. This corresponds to around 20% of the total shortening. Numerous studies have calculated a Miocene shortening of 1000 m (33% of the total shortening), along a cross section on the western part of the Grand Luberon anticline [*Combes*, 1984; *Faucher et al*., 1988;

Gidon and Pairis, 1992; *Ford and Stahel*, 1995; *Laurent et al*., 2000; *Leleu*, 2005; *Molliex et al*., 2011]. The small difference in total shortening values between our study and those of others can be explained due to the cross sections that were used to calculate the shortening, which were located in different places of the Luberon (i.e., Grand and Petit). The deformation rate varied along the Luberon anticline, from the Salon-Cavaillon fault to the MDFZ. We can observe that the total shortening increases toward the center of the Luberon anticline and decreases toward the major faults (i.e., Salon-Cavaillon Fault (SCF) and MDFZ). On the other hand, part of the deformation was clearly of Durancian age (i.e., mid-Cretaceous times), as shown by the lack of Upper Cretaceous in the majority of the study area. This lack is explained by a bulge in Provence in the mid-Cretaceous times, which was characterized by a tilting of the sedimentary series and the onset of normal faults of the bulge [*Guyonnet-Benaize et al*., 2010].

In summary, the present-day folds and thrust in the Middle Durance region result from Pyrenean deformation, which was inherited from a major Durancian prestructuration, evidenced as shown by the numerous deposits of bauxite and ochre in Provence (e.g., Allauch, Coulon, and Apt). The Alpine deformation reactivated these structures during the Miocene times (between 16 Ma and 6 Ma).

8. Conclusions

This 3-D study leads to a new characterization of the present-day 3-D geometry of the main tectonic structures in Middle Durance region and the 3-D complex geometry of the MDFZ and its relation to the E-W folds during the Mesozoic and Cenozoic times. The 3-D structural model of the Middle Durance region is relevant for kilometer-scale tectonic structures (e.g., faults and folds) with structural inheritance, and it can be compared with other basins with complex structural architectures.

This 3-D structural model has allowed us to answer unresolved questions.

1. Concerning the real 3-D geometry of the complex MDFZ: This 3-D model has shown that the MDFZ is composed of several segments that are subdivided into two fault levels, as follows: One of eight normal faults (N30°–N40°) that affected only the Paleozoic basement, with dip varying from 55° to 64° toward the west. Located above the southeastern boundary of the SE Basin, these faults present staircase geometry in the basement, with no connection to the faults that affected the Mesozoic to Cenozoic sedimentary cover, two of seven listric fault segments in the Mesozoic to Cenozoic sedimentary cover that are anchored in the Triassic evaporitic layers.
2. Concerning the relationships between the Paleozoic basement and the Meso-Cenozoic filling of the SE Basin: This 3-D model reveals a strong mechanical decoupling between the Mesozoic sedimentary cover and the Paleozoic basement, generating the complex faulting network geometry of the MDFZ, highlighting the thin-skin deformation.
3. Concerning the effective role of the MDFZ in the accommodation of this deformation and the structural relationships between this major fault and the main tectonic structures: The 3-D geometry of the fault network also reveals that the MDFZ is a transfer fault through time. This transfer fault limits folds and thrusts and modifies the fold geometry into drag, en échelon, or rectilinear axis folds, with a lateral influence zone of 7 km to 8 km.
4. Concerning the sedimentary layers and the tectonic structures involved in the deformation and the way they accommodate this deformation: The 3-D model reveals that the affected folds are fault-bend folds and fault-propagation folds. They resulted from the folding of the Mesozoic sedimentary series that was seen both parts of the MDFZ and was controlled by the following: one of the thicknesses of the sedimentary cover above the Paleozoic basement (2 km to the east and 10 km to the west) and two of the décollement levels in the sedimentary cover (three levels in the Triassic, Callovian-Oxfordian, and Valanginian units).

This study confirms that the Middle Durance geological structures (i.e., its folds and thrusts) mainly result from Pyrenean deformation that was inherited from a major Durancian prestructuration. These structures were reactivated by the Alpine deformation.

The 3-D structural model of the Middle Durance region will be used to produce a 3-D velocity model of the wave propagation for better location of seismicity. It will also be useful for seismic hazard assessment reevaluation (using both probabilistic and deterministic approaches), especially concerning extreme seismic events (e.g., stress tests), through better knowledge of the maximum length of the tectonic incidents and better understanding of the geodynamical history of the Provence.

Acknowledgments
This study was supported by the PACA region and the Cashima Research Project (funded by the French Alternative Energies and Atomic Energy Commission (CEA) and ITER). Some of the data to support this article are from the French Alternative Energies and Atomic Energy Commission (CEA). Because of security issues, the data cannot be released. The authors wish to express their gratitude to the geophysicists and structural geologists of the "Impro Durance" working group (E.M. Cushing, S. Molliex, J. Fleury, L. Bollinger, Ph. Combes, P Renoux, O. Bellier, F. Hanot, and M. Terrier) and to the working group of the College de France (X. Le Pichon, C. Rangin, and Y. Hamon). The authors wish to express their gratitude to the reviewers who greatly helped improving the quality of the present paper.

References

Arlhac, P., E. Colomb, J. Gervais, and J. Rouire (1970), Carte géologique détaillée de la France à 1/50 000, feuille 995 Pertuis, BRGM, Orléans, France.

Arnaud, H. (1981), De la plate-forme urgonienne au basin vocontien: Le Barrémo-Bedoulien des Alpes occidentales entre l'Isère et le Buëch (Vercors méridional, Diois oriental et Devoluy), Géologie alpine, Mémoire H.S. 12, 804 pp.

Arthaud, F., and P. Matte (1977), Late Paleozoic strike-slip faulting in Southern Europe and Northern Africa: Result of right-lateral shear zone between the Appalachians and the Urals, *Geol. Soc. Am. Bull.*, *8*, 1305–1320.

Baroux, E. (2000), Tectonique active en région à sismicité modérée: Le cas de la Provence (France), Apport d'une approche pluridisciplinaire, Thèse de Doctorat, 311 pp., Université Paris 6.

Baroux, E., N. Béthoux, and O. Bellier (2001), Analyses of the stress field in southeastern France from earthquake focal mechanisms, *Geophys. J. Int.*, *145*, 336–348.

Baudrimont, A. F., and P. Dubois (1977), Un Bassin Mésogéen du domaine péri-alpin: Le Sud-Est de la France, *Bull. Cent. Rech. Explor. Prod. Elf Aquitaine*, *1*, 261–308.

Belleville, J.-M., A. Pachoud, J. Savournin, J.-P. Destombes, E. Roch, P. De Peyronnet, and G. Demarcq (1966), Carte géologique détaillée de la France à 1/50 000, feuille 968 Reillanne, BRGM, Orléans, France.

Bellier, O., et al. (2007), Tectonique active de la Provence, Colloque Tectonique récente de la Provence: Rôle des couches ductiles, Collège de France, CEREGE - Europôle de l'Arbois.

Benedicto Esteban, A. (1996), Modèles tectono-sédimentaires de bassins en extension et style structural de la marge passive du Golfe du Lion (partie Nord), Sud-Est de la France, Thèse de Doctorat, 235 pp., Université Montpellier 2.

Bergerat, F. (1987), Stress field in the European platform at the time of Africa-Eurasia collision, *Tectonics*, *6*, 99–132, doi:10.1029/TC006i002p00099.

Bertrand, M. (1899), La grande nappe de recouvrement de la Basse-Provence, *Bull. Serv. Carte Geol. Fr.*, *X*(68), 397–467.

Biondi, P., O. Lerat, and J. Phillips (1992), Synthèse structurale, sédimentologique et géochimique du bassin Eocène-Oligocène de Manosque-Forcalquier (Alpes de Haute-Provence), Rep., 151 pp., IFP.

Blanc, J. J., and J. Rouire (1973), Carte géologique détaillée de la France à 1/50 000, feuille 942 Sault-de-Vaucluse, BRGM, Orléans, France.

Blanc, J. J., J. P. Masse, J. M. Triat, and J. Rouire (1975), Carte géologique détaillée de la France à 1/50 000, feuille 941 Carpentras, BRGM, Orléans, France.

Blès, J.-L., and Y. Gros (1991), Stress field changes in the Rhône Valley from the Miocene to the present, *Tectonophysics*, *194*, 265–277.

Boillot, G., L. Montardet, M. Lemoine, and B. Biju-Duval (1984), *Les Marges Continentales Actuelles et Fossiles Autour de la France*, 342 pp., Masson, Paris.

Borgomano, J., F. Hollender, C. Guyonnet-Benaize, J. Lamarche, P. Münch, L. Mocochain, F. Demory, and J. P. Masse (2010), Cartographie géologique haute résolution des unités de litho-faciès de la région de Cadarache, GSRC, Marseille, Demander réf exacte à Fabrice.

Bove, L. (1996), Proposition d'interprétation sismique sur la zone de la Moyenne Durance, Rep., IRSN.

Bove, L. (1997), Proposition d'interprétation sismique sur la zone de la Moyenne Durance, Campagne 71D. Rep., IRSN.

Bove, L. (1998), Proposition d'interprétation sismique sur la zone de la Moyenne Durance, Campagne 71D, Rep., 18 pp., IRSN.

Caumon, G., P. Collon-Drouaillet, C. Le Carlier de Veslud, V. Viseur, and J. Sausse (2009), Surface-based 3-D modelling of geological structures, *Math. Geosci.*, *41*, 927–945.

Champion, C. (1999), Déformation de la Provence occidentale depuis le Miocène. Etude structurale, utilisation de surfaces géomorphologiques marqueurs et analyse quantitative du relief, Thèse de Doctorat, 203 pp., Aix-Marseille III.

Champion, C., P. Choukroune, and G. Clauzon (2000), La déformation post-Miocène en Provence occidentale, *Geodin. Acta*, *13*, 67–85.

Chantaine, J., et al. (1996), *Carte Géologique de la France à l'Echelle du Millionième*, 6ième éd., BRGM, Orléans, France.

Chardon, D., and O. Bellier (2003), Geological boundary conditions of the 1909 Maùbesc (Provence, France) earthquake: Structure and evolution of the Trévaresse ridge anticline, *Bull. Soc. Geol. Fr.*, *174*(5), 497–510.

Choukroune, P., and M. Mattauer (1978), Tectonique des plaques et Pyrénées: Sur le fonctionnement de la faille transformante Nord-Pyrénéenne, comparaison avec les modèles actuels, *Bull. Soc. Geol. Fr.*, *7*(10), 698–700.

Choukroune, P., M. Séguret, and A. Galdeano (1973), Caractérisation et évolution structurale des Pyrénées: Un modèle de relations entre tectonique de plaques et Pyrénées, *Bull. Soc. Geol. Fr.*, *7*(15), 698–700.

Clauzon, G. (1984), Evolution géodynamique d'une montagne provençale et de son piémont: L'exemple du Lubéron (Vaucluse, France), Montagnes et Piémonts, R.G.P.S.O., Toulouse, France.

Clauzon, G., T. J. Fleury, O. Bellier, S. Molliex, L. Mocochain, and J.-P. Aguilar (2011), Morphostructural evolution of the Luberon since the Miocene (SE France), *Bull. Soc. Geol. Fr.*, *182*(2), 93–108.

Combes, P. (1984), La Tectonique récente de la Provence Occidentale: Microtectonique, caractéristiques dynamiques et cinématiques. Méthodologie de zonation tectonique et relations avec la sismicité, 192 pp., Univ. Louis Pasteur, Strasbourg, France.

Corroy, G., C. Tempier, and J.-P. Durand (1964), Evolution tectonique de la montagne Sainte-Victoire en Provence, *Bull. Soc. Geol. Fr.*, *6*(VI), 91–106.

Cushing, E. M., O. Bellier, S. Nechtschein, M. Sébrier, A. Lomax, P. Volant, P. Dervin, P. Guignard, and L. Bove (2008), A multidisciplinary study of a slow-dipping fault for seismic hazard assessment. The example of the Middle Durance Fault (SE France), *Geophys. J. Int.*, *172*, 1163–1178.

Cushing, M., and O. Bellier (2003), Faille de la Moyenne Durance: Précisions concernant le tracé en surface de la faille entre Pertuis et Château-Arnoux, Rep., 17 pp., I.R.S.N.

Cushing, M., O. Bellier, P. Volant, H. Aochi, S. Baize, and C. Berge-Thierry (2004), Recent findings integrated in seismic hazard assessment: The case study of the Durance fault, Committee on the Safety of Nuclear Installations CSNI Workshop on "Seismic Input Motions, Incorporating Recent Geological Studies" Tsukuba, Japan.

Cushing, M., S. Baize, P. Guignard, O. Bellier, L. Siame, F. Nguyen, and S. Garambois (2005), Estimation de l'aléa sismogénique d'une faille active du Sud-Est de la France: Paléosismicité de la Faille de la Moyenne Durance dans la région de Manosque, Rep., 29 pp., IRSN, CEREGE.

Debrand-Passard, S., S. Courbouleix, and M. J. Lienhardt (1984), *Synthèse Géologique du Sud-Est de la France*, vol. 125, Mémoires du B.R.GM., Orléans, France.

Denizot, G., and G. Corroy (1959), Carte géologique détaillée de la France à 1/50 000, feuille 1021 Aix-en-Provence, BRGM, Orléans, France.

Dubar, M. (1983), Stratigraphie des dépôts du Néogène supérieur et du Pléistocène du bassin de la Moyenne Durance; interprétations géodynamiques et paleogéographiques, Thèse de Doctorat, 484 pp., Univ. de Provence, Marseille, France.

Dubar, M., J.-P. Aguilar, J. Chaline, J. Michaux, and F. Semah (1998), Données chronologiques (mammifères et magnétostratigraphie) sur les dépôts plio-pléistocènes au toit du bassin de Valensole: Implications morphodynamiques, *Géol. Fr.*, *1*, 57–68.

Espurt, N., J.-C. Hippolyte, M. Saillard, and O. Bellier (2012), Geometry and kinematic evolution of a long-living foreland structure inferred from field data and cross section balancing, the Sainte-Victoire System, Provence, France, *Tectonics*, *31*, TC4021, doi:10.1029/2011TC002988.

Faucher, T., M. Gidon, J.-L. Pairis, and G. Mascle (1988), Directions de transport au front de la nappe de Digne (chaînes subalpines méridionales), *C. R. Acad. Sci. Paris D*, *306*, 227–230.

Ford, M., and U. Stahel (1995), The geometry of a deformed carbonate slope-basin transition: The Ventoux-Lure fault zone, SE France, *Tectonics*, *14*, 1393–1410, doi:10.1029/95TC02522.

Ford, M., W. H. Lickorish, and N. Kusznir (1999), Tertiary foreland sedimentation in the Southern Subalpine Chains, SE France: A geodynamic appraisal, *Basin Res.*, *11*(4), 315–336.

Gattacceca, J., A. Deino, R. Rizzo, D. S. Jones, B. Henry, B. Beaudoin, and F. Vadeboin (2007), Miocene rotation of Sardinia: New paleomagnetic and geochronological constraints and geodynamics implications, *Earth Planet. Sci. Lett.*, *258*, 359–377.

Germain, C., M. Liouville, P. de Bouchony, E. Roch, and G. Demarcq (1966), Carte géologique détaillée de la France à 1/50000, feuille 967 Cavaillon, BRGM, Orléans, France.

Gidon, M., and J.-L. Pairis (1992), Relation entre le charriage de la nappe de Digne et la structure de son autochtone dans la vallée du Bès (Alpes de Haute-Provence, France), *Eclogae Geol. Helv.*, *85*, 327–359.

Gigot, P., G. Thomel, H. Mercier, E. Colomb, M. Dubar, D. Dufay, and L. Demay (1982), Carte géologique détaillée de la France à 1/50000, feuille 943 Forcalquier, BRGM, Orléans, France.

Gisquet, F., J. Lamarche, M. Floquet, J. Borgomano, J.-P. Masse, and B. Caline (2013), 3-D structural model of composite dolomite bodies in folded area (Upper Jurassic of the Etoile massif, SE France), *AAPG Bull.*, *97*(9), 1477–1501.

Gouvernet, C., E. Colomb, J. Gervais, S. Gueirard, D. Nury, and J. Rouire (1968), Carte géologique détaillée de la France à 1/50 000, feuille 994 Salon de Provence, BRGM, Orléans, France.

Grellet, B., P. Combes, T. Granier, and H. Philip (1993), Sismotectonique de la France métropolitaine dans son cadre géologique et géophysique, *Mem. Soc. Geol. Fr.*, *1*, 164.

Guieu, G. (1968), Etude tectonique de la région de Marseille, Thèse de Doctorat, 604 pp., Université de Provence.

Guignard, P., O. Bellier, and D. Chardon (2005), Géométrie et cinématique post-oligocène des failles d'Aix et de la moyenne Durance (Provence, France), *C. R. Geosci.*, *337*, 375–384.

Guyonnet-Benaize, C. (2011), Modélisation 3D multi-échelle des structures géologiques de la région de la Faille de la Moyenne Durance (SE France), Thèse de doctorat, p. 182, Université de Provence, Académie d'Aix-Marseille I.

Guyonnet-Benaize, C., J. Lamarche, J.-P. Masse, M. Villeneuve, and S. Viseur (2010), 3-D structural modelling of small-deformations in poly-phase faults pattern. Application to the mid-Cretaceous Durance uplift, Provence (SE France), *J. Geodyn.*, *50*(2), 81–93.

Haug, M. (1925), *Les Nappes de Charriage de la Basse-Provence. Première Partie: La Région Toulonnaise*, Mémoires d'Exploration de la Carte Géologique de France, 304 pp., Paris.

Higgins, S., R. J. Davies, and B. Clarke (2007), Antithetic fault linkages in a deep water fold and thrust belt, *J. Struct. Geol.*, *29*(14), 1900–1914.

Hollender, F., et al. (2009), Deep geometry of the Middle Durance Fault system (SE of France): Reprocessing and new interpretation of reflection seismic sections, paper 130 presented at International Conference Provence 2009, Aix-en-Provence, July 6–8.

IGN (1996a), Top 25 Gréoux-les-Bains, Rians (Basses Gorges du Verdon), 1:25 000^2, IGN, Paris.

IGN (1996b), Top 25. Manosque Forcalquier (Parc Naturel Régional du Luberon), 1:25 000^2, IGN, Paris.

IGN (1998), Top 25, 1:25 000^2, IGN, Paris.

IGN (1999), Top 25. Montagne Sainte-Victoire (Aix-en-Provence, Gardanne. Trets), 1:25 000^2, IGN, Paris.

IGN (2002), Top 25 Pertuis. Lourmarin (Parc Naturel Régional du Luberon), 1:25 000^2, IGN, Paris.

Lamarche, J., A. P. C. Lavenu, B. D. M. Gauthier, Y. Guglielmi, and O. Jayet (2012), Relationships between fracture patterns, geodynamics and mechanical stratigraphy in Carbonates (South-East Basin, France), *Tectonophysics*, *581*, 231–245.

Laurent, O., J.-F. Stephan, and M. Popoff (2000), Modalités de la structuration miocène de la branche sud de l'arc de Castellane (chaînes subalpines méridionales), *Géol. Fr.*, *3*, 33–65.

Lavenu, A. P. C., J. Lamarche, A. Gallois, and B. D. M. Gauthier (2013), Tectonic versus diagenetic origin of fractures in naturally fractured carbonate reservoir analogue (Nerthe anticline, southeastern France), *AAPG Bull.*, *97*(12), 2207–2232.

Le Carlier de Veslud, C., O. Bourgeois, M. Diraison, and M. Ford (2005), 3-D stratigraphic and structural synthesis of the Dannemarie basin (Upper Rhine Graben), *Bull. Soc. Geol. Fr.*, *176*(5), 433–442.

Le Pichon, X., C. Rangin, and O. Bellier (2007), Un bassin mésozoïque déstabilisé par la distension oligocène, Colloque Tectonique récente de la Provence: rôle des couches ductiles, CEREGE - Europôle de l'Arbois.

Le Pichon, X., C. Rangin, Y. Hamon, N. Loget, J. Y. Lin, L. Andreani, and N. Flotte (2010), Geodynamics of the France Southeast Basin, *Bull. Soc. Geol. Fr.*, *181*(6), 477–501.

Leleu, S. (2005), Les cônes alluviaux Crétacé Supérieur/Paléocène en Provence: Traceurs de l'évolution morpho-tectonique des stades précoces de collision, Thèse de Doctorat, 222 pp., Université Louis Pasteur.

Lemoine, M. (1985), Structuration jurassique des Alpes occidentales et palinspatique de la Téthys ligure, *Bull. Soc. Geol. Fr.*, *8*(1), 126–137.

Lemoine, M., and P. C. De Graciansky (1988), Marge continentale téthysienne dans les Alpes Occidentales, *C. R. Acad. Sci. Paris*, *8.4*(485), 597–797.

Lemoine, M., T. Bas, A. Arnaud-Vanneau, H. Arnaud, T. Dumont, M. Gidon, P. C. De Graciansky, J. L. Rudkiewick, and P. Tricard (1986), The continental margin of Mesozoïc Tethys in the western Alps, *Mar. Pet. Geol.*, *3*, 178–199.

Lin, J. Y., and X. Le Pichon (2007), Relocalisation 3-D de la microsismicité à partir du réseau sismique IRSN de la Faille de la Moyenne Durance, Colloque Tectonique récente de la Provence: rôle des couches ductiles, CEREGE - Europôle de l'Arbois.

Lutaud, L., and G. Denizot (1963), Carte géologique détaillée de la France à 1/50 000, feuille 1020-1043 Martigues, BRGM, Orléans, France.

Maerten, L., D. D. Pollard, and F. Maerten (2001), Digital mapping of three-dimensional structures of the Chimney Rock fault system, central Utah, *J. Struct. Geol.*, *23*, 585–592.

Mallet, J. L. (1989), Discrete smooth interpolation, *ACM Trans. Graphics*, *8*, 121–144.

Mallet, J. L. (1992), Discrete smooth interpolation in geometric modeling, *Comput. Aided Des. J.*, *24*(4), 263–270.

Mallet, J. L. (2002), *Geomodelling*, 666 pp., Oxford Univ. Press, New York.

Masse, J.-P., and J. Philip (1976), Paléogéographie et tectonique du Crétacé moyen en Provence: Révision du concept d'isthme durancien, *Rev. Geogr. Phys. Geol. Dyn.*, *18*(1), 49–66.

Mennessier, G., and D. Modret (1966), Carte géologique détaillée de la France à 1/50 000, feuille 996 Tavernes, BRGM, Orléans, France.

Mennessier, G., J.-P. Caron and J. Rouire (1979), Carte géologique détaillée de la France à 1/50 000, feuille 1022 Brignoles, BRGM, Orléans, France.

Mercier, H., E. Colomb, P. Gigot, G. Mennessier, J. Gervais, J.-P. Destombes, and J. Rouire (1972), Carte géologique détaillée de la France à 1/50000, feuille [969] Manosque, BRGM, Orléans, France.
Molliex, S. (2009), Caractérisation de la déformation tectonique récente en Provence (Sud-Est France), Thèse de Doctorat, 346 pp., Université Paul Cézanne.
Molliex, S., O. Bellier, M. Terrier, J. Lamarche, G. Martelet, and N. Espurt (2011), Tectonic and sedimentary inheritance on the structural framework of Provence (SE France): Importance of the Salon-Cavaillon fault, *Tectonophysics*, *501*(1–4), 1–16.
Rangin, C., X. Le Pichon, Y. Hamon, N. Loget, and A. Crespy (2010), Gravity tectonics in the SE Basin (Provence, France) imaged from seismic reflection data, *Bull. Soc. Geol. Fr.*, *181*(6), 503–530.
Rosenbaum, G., G. S. Lister, and C. Duboz (2002), Relative motions of Africa, Iberia and Europe during Alpine orogeny, *Tectonophysics*, *359*, 117–129.
Roure, F., and B. Colletta (1996), Cenozoic inversion structures in the foreland of the Pyrenees and the Alps, in *PeriTethys Memoir 2*, edited by P. Ziegler and F. Horwath, pp. 173–210, Museum National d'Histoire Naturelle, Paris.
Roure, F., J. P. Brun, B. Colletta, and J. Van Den Driessche (1992), Geometry and kinematics of extensional structures in the Alpine foreland basin of Southeastern France, *J. Struct. Geol.*, *14*, 503–519.
Sébrier, M., L. Siame, O. Bellier, and C. Chardon (2004), Seismotectonic model for Provence (SE France), SAFE Report, project No: EVGI-2000-22005, delivrable #4.4, pp. 96–127.
Spottke, I., E. Zechner, and P. Huggenberger (2005), The southeastern border of the Upper Rhine Graben: A 3-D geological model and its importance for tectonics and groundwater flow, *Int. J. Earth Sci.*, *94*, 580–593.
Suppe, J. (1983), Geometry and kinematics of fault-bend folding, *Am. J. Sci.*, *283*(7), 684–721.
Tassy, A. (2012), Karsts côtiers et canyons sous-marins de la marge provençale au Cénozoïque: Contrôle géodynamique, eustatique, hydrologique et structural, 416 pp., Aix-Marseille, Marseille.
Tempier, C. (1987), Modèle nouveau de mise en place des structures provençales, *Bull. Soc. Geol. Fr.*, *8*(III.3), 409–628.
Terrier, M. (1991), Néotectonique de la Provence Occidentale (France): Vers une analyse multicritère des déformations récentes. Application à la classification des structures sismogènes, Thèse de Doctorat, 343 pp., Université de Provence.
Terrier, M. (2004a), Identification et classification des failles actives de la Région Provence-Alpes-Côte d'Azur. Phase 2: Analyse et synthèse des connaissances actuelles sous la forme de fiches descriptives des failles—Partie 1, *Rapport 53151*, 30 pp., B.R.G.M.
Terrier, M. (2004b), Identification et classification des failles actives de la Région Provence-Alpes-Côte d'Azur. Phase 2: Fiches descriptives des failles—Partie 2., Rapport 53151, 328 pp., B.R.G.M.
Triat, J. M., and G. Truc (1983), Le rôle des failles N50 dans la sédimentation des temps Méso et Cénozoïques et dans l'évolution tectonique du Bassin du Sud-Est (France), Rep., 425–431 pp., Elf-Aquitaine.
Villegier, M., and J. Andrieux (1987), Phases tectoniques post-Eocènes et structuration polyphasée du panneau de couverture nord provençal (Alpes externes méridionales), *Bull. Soc. Geol. Fr.*, *III*, 147–156.
Wells, D. L., and K. J. Coppersmith (1994), New empirical relationships among magnitude, rupture length, rupture width, rupture area, and surface displacement, *Bull. Seismol. Soc. Am.*, *84*(4), 974–1002.